Marine Chemistry 204 (2018) 70–85

Contents lists available at ScienceDirect

Marine Chemistry

journal homepage: www.elsevier.com/locate/marchem

Dissolved and particulate trace elements in late summer Arctic melt ponds

Chris M. Marsay[a], Ana Aguilar-Islas[b], Jessica N. Fitzsimmons[c], Mariko Hatta[d], Laramie T. Jensen[c], Seth G. John[e], David Kadko[f], William M. Landing[g], Nathan T. Lanning[c,h], Peter L. Morton[i], Angelica Pasqualini[j], Sara Rauschenberg[k], Robert M. Sherrell[l], Alan M. Shiller[m], Benjamin S. Twining[k], Laura M. Whitmore[m], Ruifeng Zhang[e,n], Clifton S. Buck[a,*]

[a] Skidaway Institute of Oceanography, University of Georgia, Savannah, GA, USA
[b] College of Fisheries and Ocean Sciences, University of Alaska Fairbanks, Fairbanks, AK, USA
[c] Department of Oceanography, Texas A&M University, College Station, TX, USA
[d] School of Ocean and Earth Science and Technology, University of Hawai'i at Manoa, Honolulu, HI, USA
[e] Department of Earth Sciences, University of Southern California, Los Angeles, CA, USA
[f] Florida International University, Applied Research Center, Miami, FL, USA
[g] Department of Earth, Ocean and Atmospheric Science, Florida State University, Tallahassee, FL, USA
[h] Department of Biology & Environmental Science, University of New Haven, West Haven, CT, USA
[i] National High Magnetic Field Laboratory, Tallahassee, FL, USA
[j] Department of Earth and Environmental Sciences, Columbia University, New York, NY, USA
[k] Bigelow Laboratory for Ocean Sciences, East Boothbay, ME, USA
[l] Department of Marine and Coastal Sciences and Department of Earth and Planetary Sciences, Rutgers University, New Brunswick, NJ, USA
[m] Department of Marine Science, University of Southern Mississippi, Stennis Space Center, MS, USA
[n] Institute of Oceanography, Shanghai Jiao Tong University, Shanghai, China

ARTICLE INFO

Keywords:
Trace elements
Biogeochemistry
Melt ponds
Arctic Ocean
GEOTRACES

ABSTRACT

Melt ponds are a prominent feature of Arctic sea ice during the summer and play a role in the complex interface between the atmosphere, cryosphere and surface ocean. During melt pond formation and development, micronutrient and contaminant trace elements (TEs) from seasonally accumulated atmospheric deposition are mixed with entrained sedimentary and marine-derived material before being released to the surface ocean during sea ice melting. Here we present particulate and size-fractionated dissolved (truly soluble and colloidal) TE data from five melt ponds sampled in late summer 2015, during the US Arctic GEOTRACES (GN01) cruise. Analyses of salinity, $\delta^{18}O$, and ^{7}Be indicate variable contributions to the melt ponds from snowmelt, melting sea ice, and surface seawater. Our data highlight the complex TE biogeochemistry of late summer Arctic melt ponds and the variable importance of different sources for specific TEs. Dissolved TE concentrations indicate a strong influence from seawater intrusion for V, Ni, Cu, Cd, and Ba. Ultrafiltration methods reveal dissolved Fe, Zn, and Pb to be mostly colloidal (0.003–0.2 μm), while Mn, Co, Ni, Cu, and Cd are dominated by a truly soluble (< 0.003 μm) fraction. Isotopically light dissolved Fe in some melt ponds suggests that photochemical and/or biologically driven redox cycling also takes place. Comparisons of particulate TE/Al ratios to mean crustal values indicate influences from lithogenic sources, including natural aerosols and/or sedimentary material, with significant enrichments for some elements, including Ni, Cu, Zn, Cd and Pb, that may result from anthropogenic aerosols, biogenic material, and/or in situ scavenging of dissolved TEs. Our results indicate that melt ponds represent a transitional environment in which some atmospherically-derived TEs undergo physical and/or chemical changes before their release to the surface ocean. As a result, the ongoing changes in sea ice areal extent, thickness, and melt season length are likely to influence the bioavailability of atmospheric TE input to the surface Arctic Ocean, with material released from snow and sea ice via melt ponds earlier in the summer and with more extensive direct deposition to the ocean surface.

* Corresponding author.
E-mail address: clifton.buck@skio.uga.edu (C.S. Buck).

https://doi.org/10.1016/j.marchem.2018.06.002
Received 4 April 2018; Received in revised form 24 May 2018; Accepted 18 June 2018
Available online 19 June 2018

1. Introduction

Melt ponds are a ubiquitous feature of sea ice during the Arctic summer and play an important role in the sea ice-albedo feedback mechanism (Curry et al., 1995). Increases in solar radiation and surface temperature in early summer cause melting of snow accumulations from the previous winter, and the meltwater then pools in depressions on top of the ice (Eicken et al., 2002; Fetterer and Untersteiner, 1998; Polashenski et al., 2017; Sankelo et al., 2010). The resulting melt ponds frequently cover 20–40% of the sea ice surface at the height of the melt season, with up to 90% coverage in some areas (Perovich et al., 2011; Polashenski et al., 2012 and references therein). As they develop, melt ponds lower the albedo of the sea ice (Curry et al., 1995; Eicken et al., 2004; Perovich et al., 2002), resulting in further localized warming and melting of the surrounding ice (Eicken et al., 2002). Surface topography, snow cover, age of the ice (first year or multi-year sea ice) and melt season duration all influence melt pond formation and development (Lüthje et al., 2006; Polashenski et al., 2017; Rösel and Kaleschke, 2012 and references therein).

Melt ponds also represent an exchange pathway linking the atmosphere, cryosphere, and surface ocean. Atmospheric transport and deposition of mineral aerosols and anthropogenic emission particles is an important delivery mechanism for numerous micronutrient and pollutant trace elements (TEs) to surface waters remote from continental margins (Duce et al., 1991; Jickells and Moore, 2015). In the Arctic, much of this deposition takes place onto sea ice, by dry deposition and in snowfall, resulting in the accumulation of particles and associated TEs in snow on top of the ice (Darby et al., 1974), before summertime melting of the snow forms melt ponds. Within these ponds, atmospherically-derived material may be exposed to changes in temperature, pH, and salinity, as well as additions of sediment or seawater-derived material released from the ice that forms the sides and bottom of the ponds (Lannuzel et al., 2016; Nürnberg et al., 1994). Eventually, the ponds drain and mix with the underlying seawater due to percolation through the connected pore structure of the sea ice, development of macroscopic flaws (e.g. seal holes, or cracks resulting from the movement of ice floes), or through loss of the underlying sea ice by melting (Fetterer and Untersteiner, 1998; Polashenski et al., 2012). Thus, melt ponds potentially represent an important biogeochemical processing step during the transfer of TEs from the atmosphere to the surface ocean in the Arctic region.

Although there have been numerous studies of the physical development of Arctic melt ponds, very few have included details of their biogeochemistry. Melt pond carbon dioxide-carbonate chemistry is known to be variable, with pH ranging from at least 6.1 to 10.8 in the Chukchi Sea and Canada Basin (Bates et al., 2014). Macronutrient concentrations are typically higher in "open" melt ponds (those with a direct connectivity to underlying seawater) than in "closed" ponds (those with low salinity and no apparent link to surface waters) (Lee et al., 2012), with concentrations low enough in the latter to limit biological productivity (Sørensen et al., 2017). Highly variable macronutrient concentration ratios have also been documented (Fernández-Méndez et al., 2015). Several studies have reported melt pond chlorophyll concentrations lower than or similar to those in underlying seawater, while melt pond algal communities have been shown to include both fresh water (from snow and sea ice) and marine species (Fernández-Méndez et al., 2015; Fernández-Méndez et al., 2014; Gradinger et al., 2005; Melnikov et al., 2002; Sørensen et al., 2017). To our knowledge, there are no published data for micronutrient or pollutant TEs other than mercury (Aspmo et al., 2006) in Arctic melt ponds.

The 2015 US GEOTRACES Arctic GN01 Section was designed to characterize the sources and transport of trace elements in the western Arctic Ocean. The field effort included melt pond sampling in order to investigate their role in the transfer of TEs between the atmosphere and surface ocean in the region, and to ascertain whether melt ponds could be used to estimate integrated atmospheric deposition over the months between summer melt periods. Here we compile measurements of a suite of dissolved and particulate TE concentrations from five melt ponds sampled during the section and analyzed by different research groups. The TEs discussed here include micronutrients (Cd, Co, Cu, Fe, Mn, Ni, V, Zn) and tracers of mineral dust/lithogenic material (Al, Fe, Ga, Ti) and other continental input (Ba). We also include Pb, which, along with Cd, Cu, Mn, Ni, V and Zn, can be enriched significantly in Arctic aerosols during the winter/spring (e.g. Gong and Barrie, 2005), and for which atmospheric deposition of anthropogenic aerosols may provide significant perturbations to the Arctic ecosystem. For a subset of these elements (Mn, Fe, Co, Ni, Cu, Zn, Cd and Pb), size fractionation analysis of the dissolved phase was carried out to determine the contributions from colloidal and truly soluble TEs, which may influence their bioavailability.

2. Methods

2.1. Sample collection and processing

The US GEOTRACES Arctic GN01 Section (hereafter GN01) was carried out on USCGC *Healy* during late summer 2015. The ship departed from Dutch Harbor, Alaska, on 9th August 2015, and the cruise track consisted of a northward transect through the Bering Strait and across the Makarov Basin to the North Pole, returning southward across the Canada Basin along 150°W, and arriving back in Dutch Harbor on 12th October 2015. Melt ponds were sampled at five of the six ice stations occupied north of 80°N during GN01, starting with Station 33 at the North Pole on 7th September, and at four subsequent stations on the southbound portion of the section, the most southerly being Station 46 (82.5°N) on 19th September (Fig. 1, Table 1). All ice stations were occupied in an area with water depths > 2000 m, and ice floes were selected for sampling based on sufficient size for safe sample collection and sufficient proximity to a paired water column station. Sea ice thickness at these stations ranged from 136 to 164 cm.

All sampling on the ice floes for TE measurements, including melt pond sampling, was conducted 30–50 m upwind of the ship. As the ice stations were occupied at high latitudes and relatively late in the summer, all melt ponds encountered at these stations had frozen over at the time of sampling, with liquid water present under 5–10 cm of ice covered by 10–15 cm of recent snow. Before sampling, surface snow was cleared away with an acid-cleaned polyethylene shovel, and a polyethylene and titanium trace metal clean coring system was used to drill through the upper layer of ice. Melt pond water samples were collected using a battery powered peristaltic pump (Pegasus Alexis) to fill acid-washed 20 L carboys (low density polyethylene – LDPE) through C-Flex tubing (Masterflex) that had been acid-cleaned with 0.1 M ultrapure HCl and thoroughly rinsed with ultrapure water before use. At each melt pond, the tubing was used as a probe to ascertain that the pond did indeed have a bottom layer of ice, although it was not possible to determine any connectivity with seawater through flaws in the ice, or the presence of a "false bottom" formed from refreezing of fresh meltwater. The tubing was then partially withdrawn, such that ~30 cm of the tubing remained in the melt pond. A few hundred milliliters of water were rinsed through the tubing before starting sample collection. Melt ponds can contain steep salinity gradients (Fernández-Méndez et al., 2014), so once sample collection began, the tubing was left in place in the melt pond, to reduce the risk of filling different carboys from different depths along any possible vertical gradient. No assessment was made regarding the presence or absence of salinity gradients in the melt ponds sampled.

Subsampling and filtration was carried out aboard ship within 3 h of sample collection, inside a plastic enclosure ("bubble") constructed for trace metal work and supplied with HEPA filtered air. Subsamples for dissolved TE analysis were taken from one 20 L carboy and were filtered through an Acropak-200 capsule filter (0.8/0.2 μm polysulfone

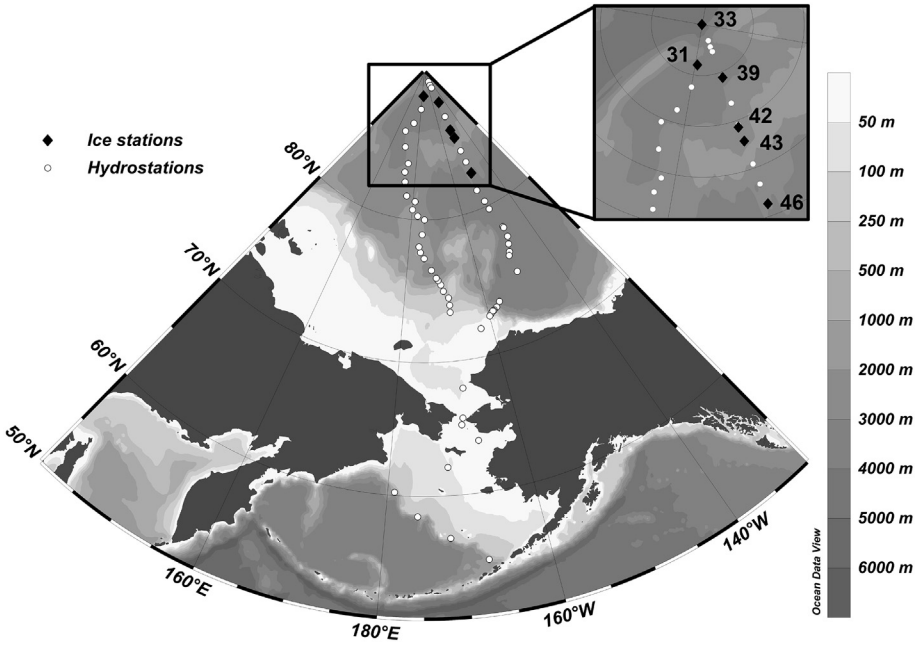

Fig. 1. Map of the US Arctic GEOTRACES GN01 section. Ice stations are shown by black diamonds. Melt ponds were sampled at all ice stations except Station 31.

membrane; Pall) into acid-cleaned LDPE bottles. For size-fractionation analyses, one of these subsamples at each station was subjected to Anopore (0.02 µm) filtration and another to cross-flow filtration (10 kDa; ~0.003 µm), as described in Fitzsimmons and Boyle (2014). Combining these two ultrafiltration approaches allowed determination of a subset of dissolved TEs in three size fractions: "truly soluble" (< 0.003 µm), "small colloidal" (0.003–0.02 µm), and "large colloidal" (0.02–0.20 µm). All filtered samples were subsequently acidified to 0.024 M with ultrapure hydrochloric acid while at sea.

Samples for particulate TE measurements were collected after gently inverting the carboy to homogenize particle distribution, then filtering 4 L of melt pond water through a 25 mm diameter Supor polyethersulfone 0.45 µm filter held in a Swinnex polypropylene filter holder, using filtered air to pressurize the carboy (Twining et al., 2015). Process blanks were also generated, by passing a similar volume of filtered (0.2 µm) seawater through Supor filters. Sample and process blank filters were digested in acid-cleaned PFA vials (Savillex) by addition of 2 mL of a solution of 4 M HCl, 4 M HNO_3, and 4 M HF (all Optima grade) and heating at 110 °C for four hours. Full details of the method are described in Twining et al. (2015).

Samples for TE analysis were also collected from snow, sea ice, and from seawater beneath the sea ice at each station. Snow samples for TE analysis were collected using an acid-cleaned polyethylene shovel to transfer the snow column into an acid-cleaned LDPE drum insert (CDF Corporation), which was held inside a plastic bucket, and which was subsequently sealed before transfer to the ship. The sample was allowed to melt at room temperature on the ship (8–10 h), and then homogenized by gentle shaking. A subsample was transferred to an acid cleaned 2 L high density polyethylene bottle under filtered air. Sea ice was collected using a trace metal clean corer. At each station, 4 ice cores (1 m in length) were collected within a 10 m^2 area. Cores were kept inside pre-cleaned custom-made plastic tube inserts that fit within the corer. These tube inserts were capped immediately after collection, and stored inside plastic bags in the ship's walk-in freezer. Cores were thawed inside custom-made melting chambers inside the plastic "bubble". Ice melt from all four melting chambers was combined and the sample homogenized by gentle shaking. Both snowmelt and ice melt samples were filtered by passing through 47 mm polyethersulfone 0.2 µm filter discs (Supor) that were loaded in in-line Teflon filter holders (Adventec).

Melt pond subsamples for salinity and oxygen isotope analysis were taken from the same 20 L carboy as the trace element samples, and subsamples for each were also taken from snow, sea ice and seawater samples. In addition, a further two 20 L carboys were filled from the same melt ponds for ^{7}Be measurements. Snow, sea ice and seawater samples were collected for ^{7}Be analysis using previously described methods (Kadko, 2000; Kadko et al., 2016).

2.2. Sample analysis

Analysis of different dissolved TEs in melt pond samples was carried out by several groups, depending on the focus of each group, as part of the collaborative GEOTRACES program. For some elements this allowed for intercomparison of data between groups. Analyses of dissolved Mn, Fe, Co, Ni, Cu, Zn, Cd, and Pb in 0.2 µm-filtered melt pond samples were carried out at the Skidaway Institute of Oceanography (SkIO) on a Perkin-Elmer NexION 300D ICP-MS following in-line preconcentration on a cation exchange column (ESI; Nobias Chelate-PA1

Table 1
Details of the melt ponds sampled during GN01, along with mean sea ice thickness, overlying snow depth and salinity of water immediately beneath the sea ice at each station.

Station #	Date sampled (UTC)	Latitude (°N)	Longitude (°E)	Melt pond salinity	Salinity of underlying water (1 m depth)	Sea ice thickness (cm)	Snow depth (cm)
33	9/7/2015	89.99	89.25	1.40	27.65	136	15
39	9/11/2015	87.77	−148.89	10.60	28.08	161	11
42	9/14/2015	85.72	−150.61	5.92	27.16	141	11
43	9/16/2015	85.16	−149.97	25.76	27.39	164	14
46	9/19/2015	82.50	−149.79	4.49	28.22	159	9

resin; (Sohrin et al., 2008)) incorporated into a seaFAST S3 flow-injection system. The analyses were calibrated using external, matrix-matched standards. Additional subsamples and size-fractionated dissolved TE samples were analyzed for the same elements at Texas A&M University (TAMU) on a Thermo-Scientific Element XR high resolution ICP-MS following offline pre-concentration on a seaFAST pico system (ESI; Nobias Chelate-PA1 resin), using a modified offline version of the isotope dilution standardized method of Lagerström et al. (2013).

Further subsamples were analyzed at the University of Southern Mississippi (USM), using a ThermoFisher Element XR ICP-MS following isotope dilution and either magnesium hydroxide coprecipitation (Ga), dilution with ultrapure water (Ba), or offline pre-concentration using a seaFAST system (V, Mn, Ni, Cu) (Hathorne et al., 2012; Jacquet et al., 2005; Shiller and Bairamadgi, 2006). Dissolved Al was measured by shipboard flow injection analysis (Measures et al., 2015; Resing and Measures, 1994) by researchers from the University of Hawai'i (UH). Stable isotope analyses of dissolved Fe, Zn, and Cd were carried out on additional subsamples at the University of Southern California (USC) using double-spike multi-collector ICP-MS, which also provides concentration data (Conway et al., 2013).

Each research group verified the accuracy of their data by concurrent analysis of seawater reference materials (Table 2). Analyses of SAFe D1 intercomparison samples carried out at both SkIO and TAMU agreed well with each other and with consensus values, although UV oxidation was not employed prior to sample processing at either institution, which likely explains the offset between measured and consensus values for Co and perhaps also Cu (Milne et al., 2010). Determinations of dissolved Al, V, Ga and Ba in the GEOTRACES GS reference sample by the relevant research groups are also shown in Table 2.

Analyses of particulate TE and phosphorus concentrations were carried out at the National High Magnetic Field Laboratory's Geochemistry Division at Florida State University (NHMFL/FSU) on a Thermo-Scientific Element 2 HR-ICP-MS, with external calibration using a matrix-matched multi-element standard (High Purity Standards, South Carolina). Digestion and analysis of three reference materials was carried out using the same method and showed good agreement with certified values (Table 3). The reference materials used were BCR-414 (plankton; Institute for Reference Materials and Measurements), and MESS-3 and PACS-2 (both marine sediment; both National Research Council of Canada).

Table 3
Reported recoveries (mean ± 1σ) of certified reference materials for particulate TE analysis (NHMFL/FSU). Typical masses digested were 10–26 mg of each reference material. Measured data are given as a percentage of certified values (*values in parentheses are based on uncertified values from GeoReM (http://georem.mpch-mainz.gwdg.de) due to a lack of certified values*). Recoveries from CRMs were not used to make corrections to melt pond data.

	IRMM BCR-414	*n*	NRCC MESS-3	*n*	NRCC PACS-2	*n*
Al	*(85% ± 7%)*	5	99% ± 5%	5	95% ± 2%	4
Ti	*(64% ± 14%)*	4	93% ± 6%	5	99% ± 4%	4
V	94% ± 4%	5	89% ± 3%	5	92% ± 8%	4
Mn	79% ± 4%	5	93% ± 5%	5	95% ± 1%	4
Fe	94% ± 2%	5	96% ± 4%	5	101% ± 1%	4
Co	95% ± 1%	5	88% ± 2%	5	96% ± 6%	4
Ni	93% ± 3%	5	93% ± 2%	5	94% ± 2%	4
Cu	92% ± 1%	5	98% ± 7%	5	96% ± 3%	4
Zn	89% ± 10%	5	91% ± 5%	5	99% ± 5%	4
Cd	63% ± 15%	5	109% ± 3%	5	90% ± 2%	4
Ba	*(60% ± 24%)*	5	*(63% ± 22%)*	5	*(100% ± 8%)*	4
Pb	87% ± 29%	5	88% ± 10%	5	103% ± 7%	4
P	*(102% ± 3%)*	5	107% ± 3%	5	111% ± 4%	4

Samples of melt ponds, snow, sea ice, and surface seawater were processed for ^{7}Be measurements using established methods (Kadko, 2000; Kadko et al., 2016). Oxygen isotope ratios ($H_2{}^{18}O/H_2{}^{16}O$) were measured at Columbia University's Lamont Doherty Earth Observatory using a Picarro L2130-i Cavity Ring-Down Spectroscopy (CRDS) analyzer, following the method and data processing described by Walker et al. (2016). Oxygen isotope data are reported as $\delta^{18}O$, which represents the per mil deviation of the $^{18}O/^{16}O$ ratio from that of Vienna Standard Mean Ocean Water (VSOW-2). Analytical precision is approximately ± 0.025‰ (Pasqualini et al., 2017). Salinity measurements were carried out at sea by members of the Oceanographic Data Facility of Scripps Institute of Oceanography, using a Guildline Autosal 8400B salinometer.

3. Results

Melt pond salinity measurements ranged from 1.4 to 25.8 (Table 1), indicating varying degrees of seawater influence in the ponds. Similarly, melt pond $\delta^{18}O$ ranged from −5.28‰ to −4.38‰ (see supplementary materials; no measurement was made at Station 33), reflecting

Table 2
Reported values (mean ± 1σ) of intercomparison samples analyzed at each institution contributing dissolved TE concentration data during this study, along with the most recent consensus values (www.geotraces.org). Consensus values are for SAFe D1 for elements analyzed at SkIO and TAMU, and for GEOTRACES GS for elements analyzed at UH and USM. Values are given in nmol/kg to match reported consensus data. (*nd* = not determined).

	SAFe D1 consensus (nmol/kg)	SkIO values (nmol/kg)	*n*	TAMU values (nmol/kg)	*n*
dFe	0.67 ± 0.04	0.73 ± 0.04	6	0.70 ± 0.02	8
dMn	*0.35*[a]	0.41 ± 0.01	6	0.39 ± 0.02	7
dCo	0.045 ± 0.005	0.032 ± 0.001	6	0.032 ± 0.002	8
dNi	8.58 ± 0.26	9.34 ± 0.18	6	8.81 ± 0.18	7
dCu	2.27 ± 0.11	2.04 ± 0.05	6	2.22 ± 0.12	7
dZn	7.40 ± 0.35	7.68 ± 0.09	6	7.52 ± 0.07	7
dCd	0.991 ± 0.031	1.046 ± 0.009	3	1.005 ± 0.017	8
dPb	0.028 ± 0.003	0.022 ± 0.002	6	0.023 ± 0.001	8

	GEOTRACES GS consensus (nmol/kg)	UH values (nmol/kg)	*n*	USM values (nmol/kg)	*n*
dAl	27.5 ± 0.2	28.85 ± 1.12	2	*nd*	–
dV	*nd*[b]	*nd*	–	34.6 ± 0.5	16
dGa	*nd*[b]	*nd*	–	0.046 ± 0.004	6
dBa	*nd*[b]	*nd*	–	43.7 ± 1.0	19

[a] Not enough reported dMn data for a consensus mean and standard deviation.
[b] Consensus values not yet available for dV, dGa and dBa, but USM values were in close agreement with other laboratories during intercalibration exercises.

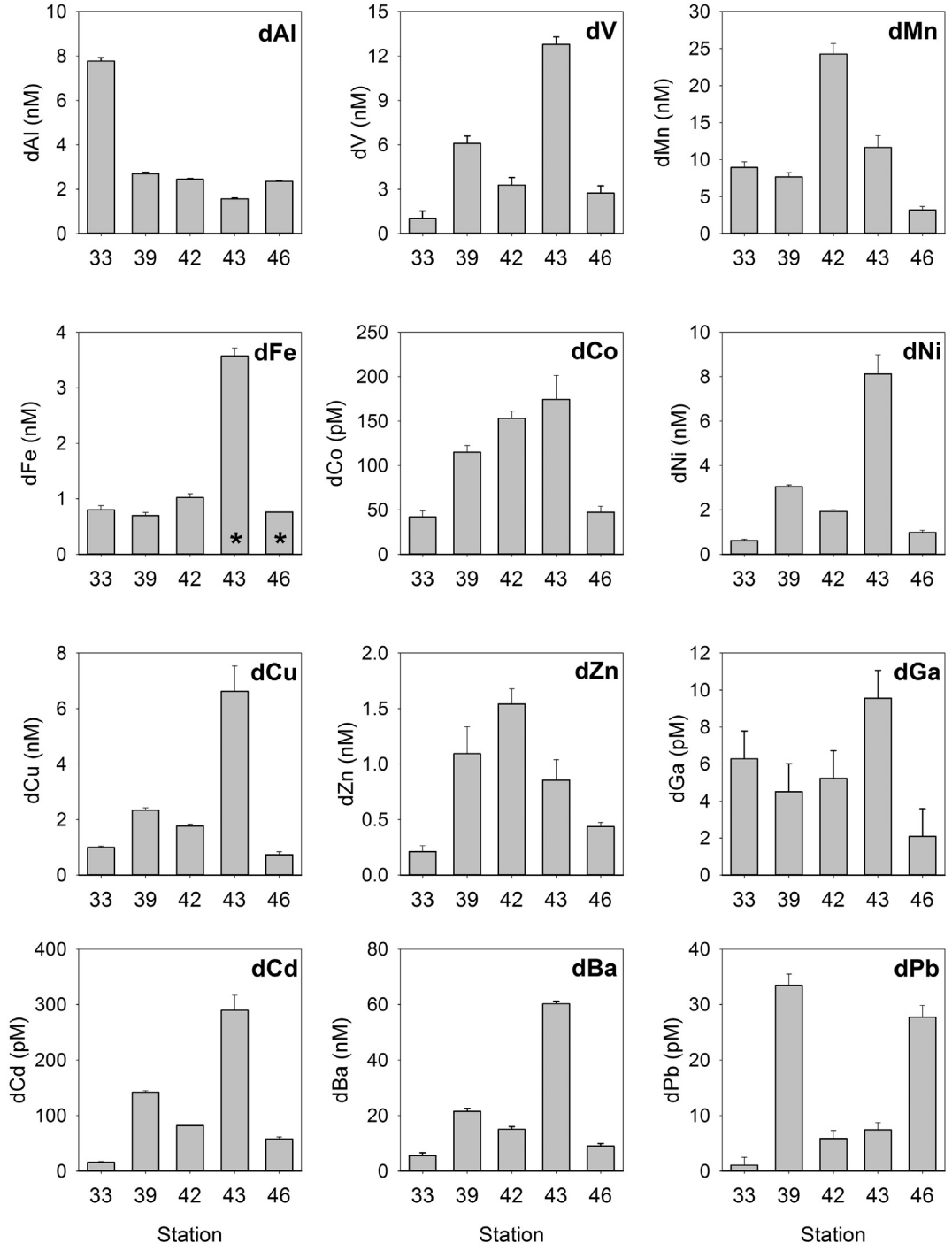

Fig. 2. Melt pond dissolved (< 0.2 μm) TE concentrations. Concentrations for dMn, dFe, dCo, dNi, dCu, dZn, dCd and dPb are SkIO data (except where * denotes TAMU data). UH data is shown for dAl. Concentrations of dV, dGa and dBa are USM data. Concentrations are shown in nM, except dCo, dGa, dCd and dPb (all pM). Error bars represent ± 1σ from replicate analyses of the same subsample for SkIO data or method precision for UH and USM data. Data for dTi are not available.

a combination of sources for the pond water (Kadko and Swart, 2004). The ^{7}Be activity measured in melt pond samples ranged from 2300 dpm/m^{3} at Station 43 to 11,200 dpm/m^{3} at Station 33 (see supplementary materials), which is a similar range to previous melt pond ^{7}Be measurements (Eicken et al., 2002; Kadko et al., 2016). This compared to mean (± 1σ) ^{7}Be activities in snow, sea ice, and surface seawater of 25,900 ± 8900 dpm/m^{3}, 1700 ± 670 dpm/m^{3} and 85 ± 24 dpm/m^{3}, respectively (see supplementary materials).

Dissolved TEs (denoted by dFe, dMn, etc.) in the five melt ponds were measured at pM to nM concentrations (Fig. 2). Analyses carried out on separate subsamples at different institutions generally gave very good agreement (see Table S1). In the following discussion, we use SkIO data except for dissolved TEs not measured at that institution – dAl (UH), dV, dGa, and dBa (all USM) – and dFe data from Stations 43 and 46, for which the SkIO data was notably lower than TAMU and USC data (TAMU data are used).

While the differences in dFe concentration between the SkIO and TAMU and USC subsamples for Stations 43 and 46 may indicate contamination of the TAMU and USC subsamples from these stations, our conclusion is that the higher concentrations are more accurate. Evidence for this comes from a lack of similarly elevated concentrations of other contamination-prone TEs (such as dZn) in these samples; the

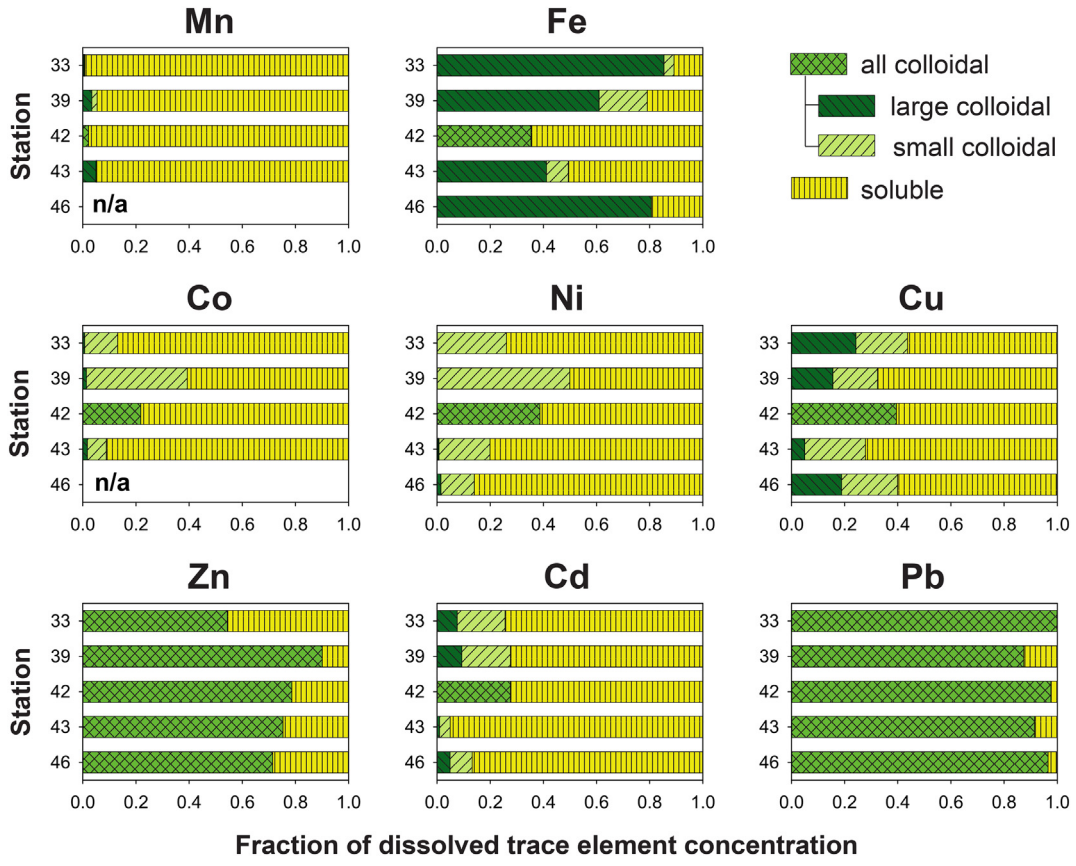

Fig. 3. Size partitioning of melt pond dissolved trace element samples between large colloidal (0.02–0.2 μm), small colloidal (0.003–0.02 μm) and soluble (< 0.003 μm) size fractions. Each is expressed as a fraction of the dissolved TE concentration. Dissolved Zn and Pb for each sample, and all dissolved TEs for Station 42, are split into a soluble fraction and only one combined colloidal fraction (0.003–0.2 μm). Size fractionation analysis was not carried out for dMn and dCo at Station 46.

good agreement between TAMU and USC data (e.g. 3.57 nM and 3.47 nM, respectively, at Station 43, compared to 0.91 nM for SkIO); and the dFe concentration and δ^{56}Fe at the high salinity Station 43 being similar to those in under-ice seawater at the same station (R. Zhang, pers. comm.). The low dFe values from SkIO for Stations 43 and 46 remain unexplained, but are restricted to those two measurements. Reanalysis of the SkIO subsamples at TAMU gave numbers in agreement with the original SkIO data, ruling out an analytical issue at SkIO. However, given the arguments above, data from the TAMU subsamples are used here.

Size-partitioning studies of filtered melt pond samples allowed concentrations of dMn, dFe, dCo, dNi, dCu, dZn, dCd, and dPb to be separated into soluble (< 0.003 μm) and colloidal (0.003–0.2 μm) fractions, with the latter subdivided into small (0.003–0.02 μm) and large (0.02–0.2 μm) colloids for all except dZn and dPb (Fig. 3). This revealed dMn, dCo, dNi, dCu and dCd to be mostly (> 50%) soluble, while dZn and dPb were predominantly colloidal, and dFe size partitioning varied between melt ponds. No size partitioning was measured for dAl, dV, dGa, or dBa.

Melt pond particulate TE concentrations (hereafter referred to as pFe, pMn, etc.) were also measured in the picomolar to nanomolar range (Fig. 4, Table S2). The highest particulate concentrations for several elements (pAl, pTi, pV, pMn, pFe, pCo, and pPb) were measured at Station 33, exceeding those for all other stations by an order of magnitude in some cases (Fig. 4).

4. Discussion

4.1. Sources of melt pond waters and trace elements

Melt ponds are formed by melting of snow that has accumulated on top of sea ice through the previous winter, and so can potentially be used to estimate integrated atmospheric deposition during the months prior to their formation. However, as they develop they receive additional brines and meltwater released through melting of the sea ice that forms the perimeter of the pond, and by exchange with the underlying seawater through various mechanisms, including percolation and the development of macroscopic flaws in the ice (Eicken et al., 2002; Fetterer and Untersteiner, 1998; Lee et al., 2012; Polashenski et al., 2012). Salinity measurements of the five melt ponds sampled during GN01 (Table 1) indicate varying contributions of seawater, with the greatest at Station 43, where the melt pond salinity (25.8) was close to that of water collected directly beneath the sea ice (27.4). This, along with the timing of the melt pond sampling in mid-September, indicates that the melt ponds sampled during GN01 were more typical of late summer ponds and more likely to have had contributions from additional sources beyond just melted snow. Thus, any melt pond TE content derived from atmospheric deposition since the previous melt period would likely have been added to from other sources and/or altered during the lifetime of the melt ponds.

Using a combination of salinity, δ^{18}O, and ^{7}Be measurements for each melt pond, together with end-member values for surface seawater, sea ice and snow, we calculated the fraction that each of these three sources contributed to the water content of each melt pond (see supplementary material). The results (Table 4) suggest that seawater contributed ~80% of the melt pond volume at Station 43, while melting

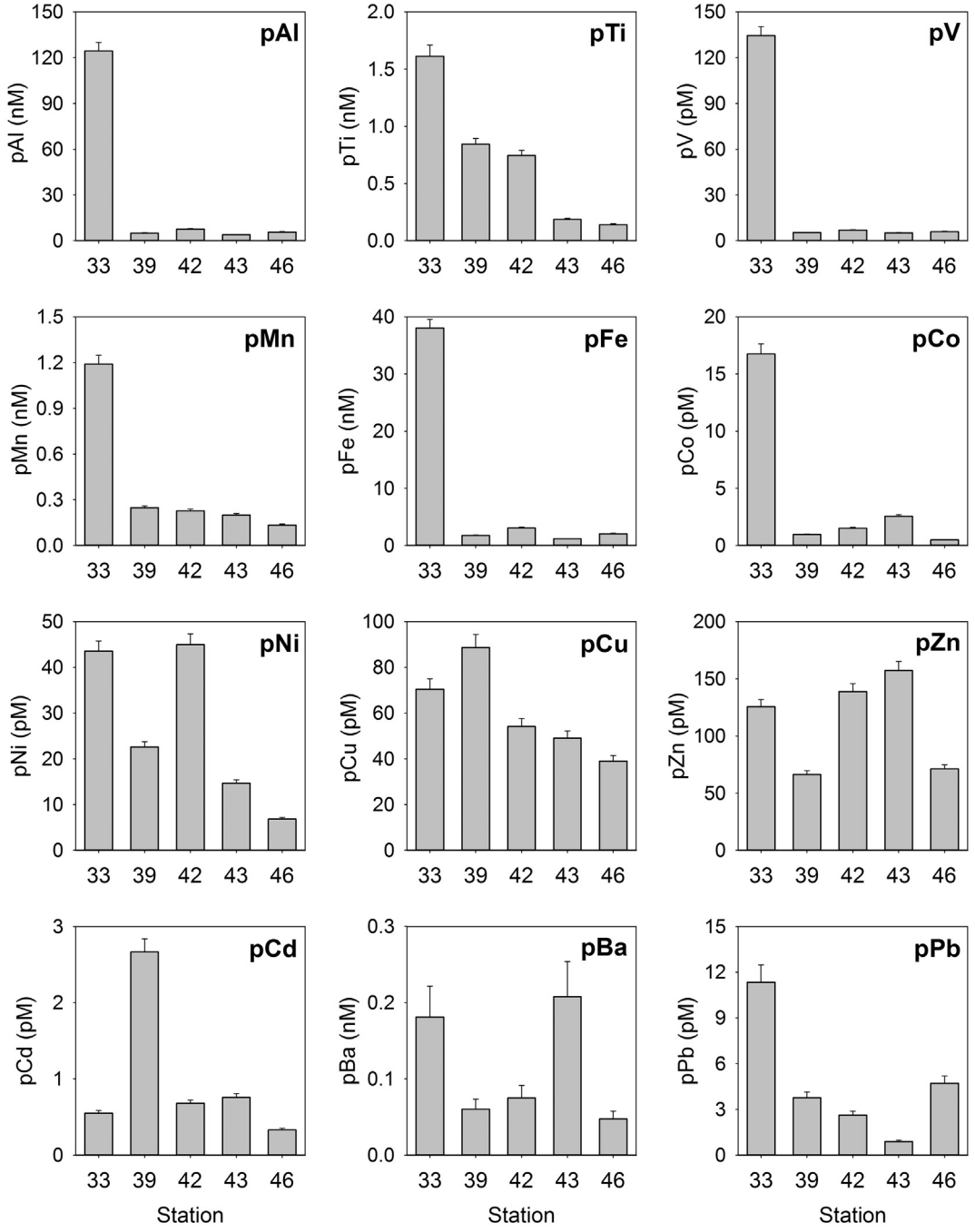

Fig. 4. Melt pond particulate (> 0.45 μm) TE concentrations by station. Concentrations are in nM for pAl, pTi, pMn, pFe and pBa, and in pM for pV, pCo, pNi, pCu, pZn, pCd and pPb. Error bars are ± one standard deviation, based on the relative standard deviation calculated from replicate digestions and analysis of MESS-3 reference material. Particulate Ga data are not available.

Table 4
Percentage contributions to melt pond volume from snow (F_{snow}), seawater (F_{sw}) and sea ice (F_{ice}). Derivations are outlined in supplementary material.

Station	Salinity	F_{snow}	F_{sw}	F_{ice}
33	1.40	94%	4%	2%
39	10.60	21%	25%	54%
42	5.92	24%	9%	67%
43	25.76	21%	79%	0%[a]
46	4.49	20%	3%	77%

[a] $F_{ice} < 1\%$.

sea ice made the dominant contribution to melt pond water at Stations 39, 42 and 46. Only at Station 33 did snowmelt represent the dominant contribution to melt pond volume (94%), with only a 20–25% contribution from snowmelt calculated for the other melt ponds (Table 4).

Based on this apportionment, the TE content of late-summer melt ponds, such as those sampled during GN01, is likely to be the product of multiple sources, which are summarized in Fig. 5. Mature melt ponds are likely to have received TE inputs by direct atmospheric deposition during summer, as well as the input of atmospherically derived TEs through the initial melting and pooling of snow from the previous winter, and are also likely to have received dissolved and particulate TEs by their release from melting of the sea ice perimeter. Dissolved and particulate materials become incorporated into sea ice during its

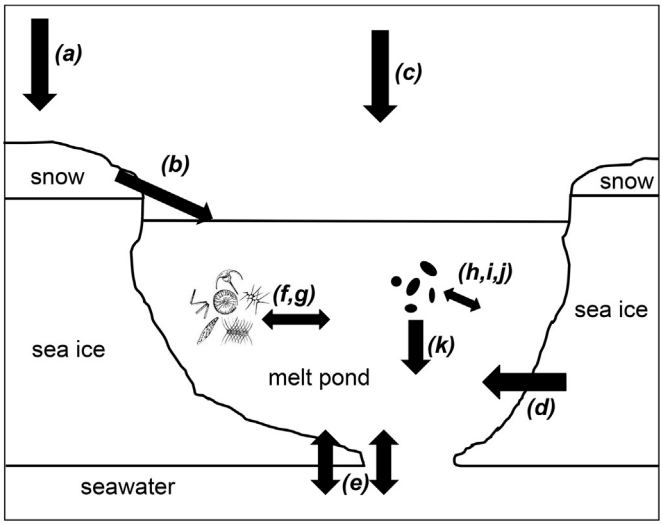

Fig. 5. Schematic summary of inputs and processes potentially influencing dissolved and particulate TE concentrations in melt ponds: *(a)* snowfall and dry atmospheric deposition onto sea ice, *(b)* drainage of snowmelt to form melt ponds, *(c)* direct atmospheric deposition during the melt season, *(d)* inputs from melting of the surrounding sea ice, *(e)* exchange with surface seawater through porous sea ice and macroscopic flaws, *(f)* biological uptake, *(g)* release/remineralization from biogenic material, *(h)* in situ precipitation, *(i)* scavenging of dissolved TEs onto particles, *(j)* dissolution of TEs from particles, *(k)* sinking of particles to the bottom of the melt pond or to the surface ocean.

formation (Janssens et al., 2016), and in the Arctic this can include contributions from fluvial inputs and resuspended shelf sediments that are then transported throughout the Arctic Ocean by the Transpolar Drift (Eicken et al., 2005; Nürnberg et al., 1994; Wegner et al., 2017). Exchange of material with the underlying seawater also becomes increasingly likely as the summer progresses.

In addition, it might be expected that TEs in melt ponds are subject to internal cycling processes. Removal of dissolved TEs to the particulate phase may occur by biological uptake, scavenging onto particles, or by in situ mineral formation as the melt pond temperature and salinity change. Conversely, remineralization of biogenic material and dissolution from aerosols or sedimentary inclusions could transfer particulate TEs to the dissolved phase, while particles will also settle to the bottom of the pond over time.

4.2. Melt pond dissolved trace elements

Melt pond concentrations of dV, dNi, dCu, dCd, and dBa all showed statistically significant positive correlations with salinity and with each other (Fig. 6). From this we infer that the degree of seawater influence on the melt ponds was the main factor controlling dissolved concentrations of these elements. This inference is supported by comparison of the concentrations of these dissolved TEs in snow, sea ice and near-surface seawater collected at the same stations (Aguilar-Islas and Rember, 2017). These data, summarized in Table 5, show that for each of these five elements, the average dissolved TE concentrations were significantly higher in seawater than in sea ice, with the lowest concentrations in snow.

Indeed, when we estimate the average expected concentration of each of these elements in the melt ponds using their mean concentrations in the three end-members and the percentage contributions to melt pond volumes by those end-members (Table 4), the modeled values come out within 15–30% of the average measured concentrations in the melt ponds (Table 5). Given that the calculations rely on independent data (TEs, salinity, and $\delta^{18}O$ or ^{7}Be) in snow, sea ice, seawater and melt ponds this agreement is remarkable. We attribute the slight underestimation of each of the five dTEs by these calculations to dissolution from aerosols during summertime direct atmospheric deposition to the melt ponds and/or to seasonal differences in TE content of snow between that collected during GN01 and the snow that initially formed the melt ponds. Snowfall over the previous fall to spring period is expected to have had a higher anthropogenic aerosol content than the fresher snow collected during GN01, due to the greater prevalence of Arctic Haze in the winter and early spring (Barrie and Hoff, 1985; Ström et al., 2003; Tunved et al., 2013). Winter/spring snow would therefore be expected to have contained higher dissolved TE concentrations than our snow samples for some elements. However, as snowmelt only contributed 20–25% of the volume for four of the five melt ponds sampled, this seasonal difference should not affect the modeled melt pond dTE concentrations significantly.

Of these five TEs, size partitioning was analyzed for dNi, dCu and dCd, and revealed in each case that the soluble (< 0.003 μm) size fraction made the greatest contribution (50–95%) to melt pond concentrations. Most of the remaining dNi and dCd was associated with small colloids, while the remaining dCu was relatively evenly split between small and large colloids (Fig. 3). Melt pond dCu size partitioning was similar to that in all three end-members, but melt pond dNi and dCd were both intermediate between seawater (low colloidal contributions) and snow and sea ice (higher colloidal contributions) (Lanning et al., 2017). Thus, as the melt pond inventories mix with seawater, it appears that colloidal contributions of dNi and dCd released from snow and sea ice are lost or at least diluted under increasing influence from seawater with higher concentrations but lower colloidal contributions.

Dissolved cadmium stable isotope data ($\delta^{114}Cd$) for the melt ponds averaged +0.49 ± 0.13‰ for all ponds except at Station 33 (Fig. 6), in agreement with the notion that near-surface seawater ($\delta^{114}Cd$ = +0.53 ± 0.04‰; Table 5) contributed the majority of melt pond dCd. In contrast, melt pond $\delta^{114}Cd$ for Station 33 and $\delta^{114}Cd$ in the single snow sample with enough dCd for isotope analysis (+0.06‰ and +0.02‰, respectively) were both much lighter than seawater values. These values are similar to the $\delta^{114}Cd$ of crustal material (John et al., 2017), suggesting an aerosol source for the small amount of dCd present in each case. Overall, measured melt pond $\delta^{114}Cd$ values agree very well with the modeled values calculated using the three end-member dCd concentration and $\delta^{114}Cd$ data, suggesting that simple mixing of the three sources controls $\delta^{114}Cd$.

There are also indications of positive relationships between melt pond salinity and concentrations of dCo and dGa, though in each case there is no statistically significant correlation (Fig. 6). Concentrations of both dCo and dGa in the surrounding snow and sea ice were again lower than those measured in near-surface seawater and generally lower than melt pond concentrations (Table 5), suggesting that seawater was the dominant but not sole influence on melt pond concentrations for these elements. Furthermore, dCo resembled dNi and dCd in having a modest colloidal fraction (averaging 17%) in melt ponds (Fig. 3), with similar colloidal contributions in snow (22%) and sea ice (16%) and a lower colloidal contribution in surface seawater (6%). It should however be noted that all dCo data discussed here represent samples that were not treated with UV-oxidation and so likely underestimate dCo chelated by strong organic ligands (e.g. Milne et al., 2010). For dGa, which has been proposed as an alternative to aluminum as a tracer of dust input (Shiller and Bairamadgi, 2006), the apparent relationship with salinity is driven by a high concentration in the most saline melt pond, while snow and sea ice sources may have had more influence on melt pond concentrations than for the TEs previously discussed. For example, the Station 33 melt pond, with ~95% snowmelt contribution by volume and lowest salinity, had the second highest dGa concentration (Figs. 2 and 6), suggesting a significant contribution from dissolution of atmospheric dust introduced with snowmelt at that station.

There is no clear relationship between melt pond dFe and salinity. The melt pond at Station 43, which had a much higher dFe

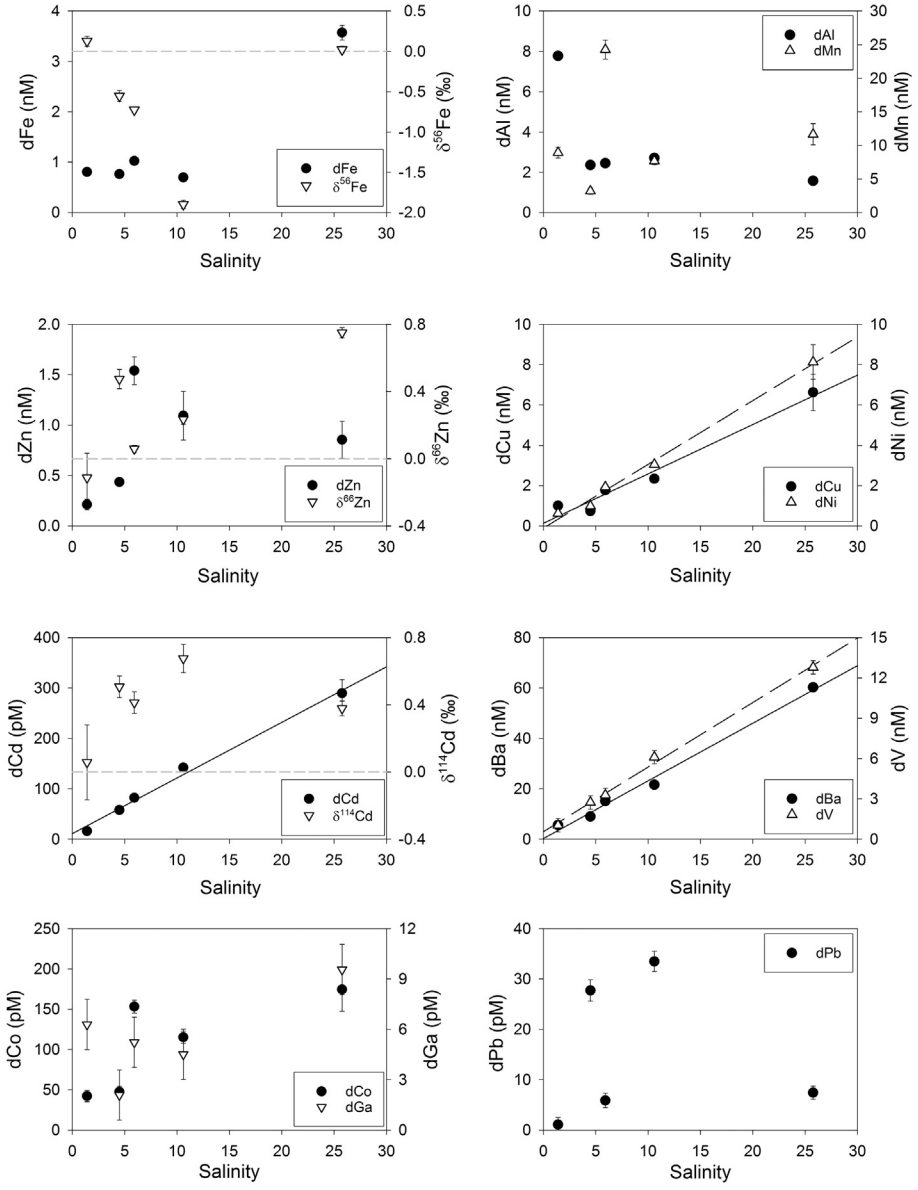

Fig. 6. Melt pond dissolved TE concentrations and δ^{56}Fe, δ^{66}Zn and δ^{114}Cd data plotted against melt pond salinity. Gray dashed horizontal line on isotope plots indicates 0‰. Where a significant ($p < 0.05$) correlation exists between concentration and salinity, a linear regression line is shown.

concentration (3.5 nM) and higher salinity than any other melt pond, had a similar dFe concentration to the underlying seawater at that station (~4.0 nM). Without this value, melt pond dFe averaged 0.8 ± 0.1 nM, with no trend with increasing salinity (Fig. 6). Furthermore, this average is lower than average concentrations measured in snow, sea ice, or seawater. A comparison of measured and modeled melt pond dFe concentrations suggests a general loss of dFe within melt ponds, relative to the three sources (Table 5).

Three potential processes could explain a loss of dFe in melt ponds compared to its sources: aggregation of colloids, scavenging onto particles, or biological uptake. Size partitioning of melt pond dFe was more variable than that for the elements previously discussed (Fig. 3). The colloidal contribution to dFe was 83 ± 5% at Stations 33, 39 and 46, but only 35% and 49% at Stations 42 and 43, respectively. However, with melt pond salinities of 5.9 and 25.8 at these latter two stations, their dFe size partitioning cannot be explained simply as a result of melt pond sourcing from seawater or fresh water. The one pattern that remained constant across the melt ponds was the dominance of large colloids within the colloidal fraction; they comprised between 40% and 85% of total dFe at the four stations where colloids were split into two size classes. Colloidal Fe also represented the largest fraction of dFe in snow (79 ± 16%) and sea ice (65 ± 10%), and was lower but significant in seawater (38 ± 14%) (Lanning et al., 2017). Thus, with significant colloidal fractions and similarly high dFe concentrations in snow, sea ice and seawater, the relatively low melt pond dFe concentrations may represent a loss from the colloidal fraction to the particulate phase by aggregation and/or scavenging processes in the melt ponds as temperature and salinity changed. This process would likely be enhanced by the presence of particles also introduced with snowmelt.

Removal of dFe by biological uptake within melt ponds cannot be ruled out. However, based on measured non-crustal particulate phosphorus concentrations and measured ice algal TE/P ratios (Table 6; see Section 4.3.2), biological uptake would likely account for only a minor uptake of dFe (and also dissolved Co, Ni, Cu and Zn) relative to measured dissolved TE concentrations. However, the full effect of this potential mechanism cannot be calculated without a thorough inventory of fresh algal material and organic aggregates that may have settled on

Table 5
Comparison of melt pond dissolved TE concentrations and stable isotope ratios to those in snow, sea ice and near surface seawater. Also shown are average modeled melt pond concentrations, based on contributions from snow, sea ice and seawater end-members (as reported in Table 4). All values are mean ± one standard deviation.

	Snow (n = 6)	Sea ice (n = 6)[a]	5 m depth seawater (n = 6)	Melt ponds (n = 5)	Modeled melt ponds (n = 5)
dTE concentrations (nM)					
Al	3.0 ± 1.7	5.4 ± 2.8	1.0 ± 0.3	3.4 ± 2.5	3.5 ± 1.4
V	0.22 ± 0.25	1.8 ± 1.5	14.7 ± 3.1	5.2 ± 4.6	4.3 ± 4.4
Mn	1.7 ± 1.7	6.0 ± 4.2	5.2 ± 1.3	11.1 ± 7.9	4.3 ± 1.3
Fe	3.6 ± 2.9	1.1 ± 1.0	3.0 ± 1.3	1.4 ± 1.2	2.5 ± 0.8
Ni	0.12 ± 0.18	0.75 ± 0.47	8.1 ± 0.6	2.9 ± 3.1	2.3 ± 2.4
Cu	0.30 ± 0.22	0.67 ± 0.44	6.4 ± 0.9	2.5 ± 2.4	1.9 ± 1.9
Zn	11.3 ± 3.8	3.2 ± 1.7	0.80 ± 0.32	0.83 ± 0.53	5.5 ± 3.0
Ba	0.8 ± 1.5	6.8 ± 4.5	68 ± 2	22 ± 22	19 ± 20
dTE concentrations (pM)					
Co[b]	20 ± 25	45 ± 20	158 ± 60	106 ± 60	63 ± 40
Ga	2.3 ± 1.4	2.3 ± 1.1	7.2 ± 1.1	5.5 ± 2.7	3.4 ± 1.6
Cd	3.5 ± 2.0	34.9 ± 21.8	288 ± 9	117 ± 106	85 ± 86
Pb	48 ± 38	35 ± 22	1.8 ± 1.3	15 ± 14	32 ± 13
dTE stable isotope ratio (‰)					
δ^{56}Fe	−0.48 ± 0.09	−0.61 ± 0.35	−0.22 ± 0.51	−0.61 ± 0.81	−0.45 ± 0.10
δ^{66}Zn	0.10 ± 0.04	−0.03 ± 0.05	0.76 ± 0.10	0.28 ± 0.34	0.10 ± 0.08
δ^{114}Cd	0.02[c]	0.20 ± 0.36	0.53 ± 0.04	0.41 ± 0.23	0.43 ± 0.10

[a] Each sample represents four sea ice cores combined to make a homogenized sample.
[b] Dissolved Co data are from non-UV-oxidized samples and therefore represent minimum values.
[c] Only one determination of δ^{114}Cd made in snow samples due to low concentrations.

the bottom of the ponds.

Iron stable isotope data are also indicative of the active cycling of Fe within melt ponds, as well as the influence of the different sources. The low salinity melt pond at Station 33 had δ^{56}Fe of +0.13‰, close to crustal values (+0.09‰; Beard et al., 2003), while δ^{56}Fe for the high salinity, high dFe Station 43 melt pond was close to that of near-surface seawater at that station (+0.06‰). At the mid-salinity melt ponds where melting sea ice dominated contributions to melt pond water, dissolved δ^{56}Fe was isotopically light, particularly at Station 39 where melt pond δ^{56}Fe (−1.90‰) was lighter than any measurements made in snow (−0.38‰ to −0.61‰) or sea ice (−0.17‰ to −1.10‰). Either biological or chemical processes could be invoked to explain the low δ^{56}Fe values observed at intermediate salinities. For example, large Fe isotope fractionations are typically associated with redox processes, with Fe(II) species typically having lighter δ^{56}Fe (Welch et al., 2003). Thus, low δ^{56}Fe could reflect photochemical or biological reduction of Fe within the ice and melt ponds to produce a pool of isotopically light dissolved Fe(II) (Ellwood et al., 2015), which could persist in the dissolved phase even after subsequent oxidation of Fe(II) back to Fe(III). Photochemistry is certainly a credible candidate for such transformations within melt ponds, as the material is exposed to long daylight hours during the Arctic summer, and their shallow depth means that even particulate material at the bottom of melt ponds receives light with relatively little attenuation from surface irradiance. However, this would be expected to increase the dFe concentration in melt ponds relative to sources and so cannot be the only mechanism influencing melt pond dFe concentration and δ^{56}Fe.

Scavenging is another mechanism that could produce low δ^{56}Fe signatures at intermediate salinities. Lower dissolved δ^{56}Fe values are typically observed in the deep chlorophyll maximum in the oceans, reflecting either biological uptake of heavy Fe isotopes or passive scavenging (Conway and John, 2015; Conway and John, 2014), and similar processes could be at work in melt ponds. Scavenging has also been observed to alter dissolved δ^{56}Fe during mixing of fresh and saline waters in estuaries, though previous studies have either found preferential loss of lighter isotopes during mixing (Escoube et al., 2009), or suggested another source of Fe within the estuary, such as anoxic sediments (de Jong et al., 2007). In this study, the fact that sea ice δ^{56}Fe is also relatively light suggests that scavenging during a change in melt pond salinity is not the mechanism responsible and points more to photochemical or biological influences.

Melt pond concentrations of dAl, dMn, dZn and dPb also showed no

Table 6
Non-crustal pTE/pP ratios (mmol/mol) calculated for each melt pond, with the percentage contribution of non-crustal pTE to total pTE shown in brackets. Also shown are ranges (lower and upper quartiles) of TE/P measured in phytoplankton cells in sea ice collected from Stations 33, 42, and 43, and ranges of TE/P ratios for phytoplankton cells reported in Twining and Baines (2013). (*nd* = not determined).

	Mn	Fe	Co	Ni	Cu	Zn	Cd
Station 33	63	1023	0.83	2.5	4.7	6.9	0.04
	(62%)	*(31%)*	*(58%)*	*(67%)*	*(77%)*	*(64%)*	*(93%)*
Station 39	10	30	0.03	0.9	3.7	2.7	0.11
	(93%)	*(41%)*	*(71%)*	*(97%)*	*(99%)*	*(97%)*	*(100%)*
Station 42	10	72	0.05	2.1	2.6	6.6	0.03
	(88%)	*(48%)*	*(71%)*	*(98%)*	*(98%)*	*(98%)*	*(100%)*
Station 43	14	26	0.18	1.1	3.6	11.6	0.06
	(93%)	*(30%)*	*(91%)*	*(97%)*	*(99%)*	*(99%)*	*(100%)*
Station 46	9	70	0.01	0.5	3.1	5.7	0.03
	(84%)	*(41%)*	*(33%)*	*(90%)*	*(98%)*	*(97%)*	*(100%)*
Sea ice algae range	0.2–3.1	4.5–11.9	0.01–0.08	0.02–0.11	0.16–0.64	1.0–4.1	*nd*
Twining and Baines (2013)[a]	0.2–5	1–31	0.01–0.2	0.2–8	0.2–2.0	1–16	0.02–1.3

[a] Ranges cover values from Table 2 and Fig. 3 of Twining and Baines (2013) review article.

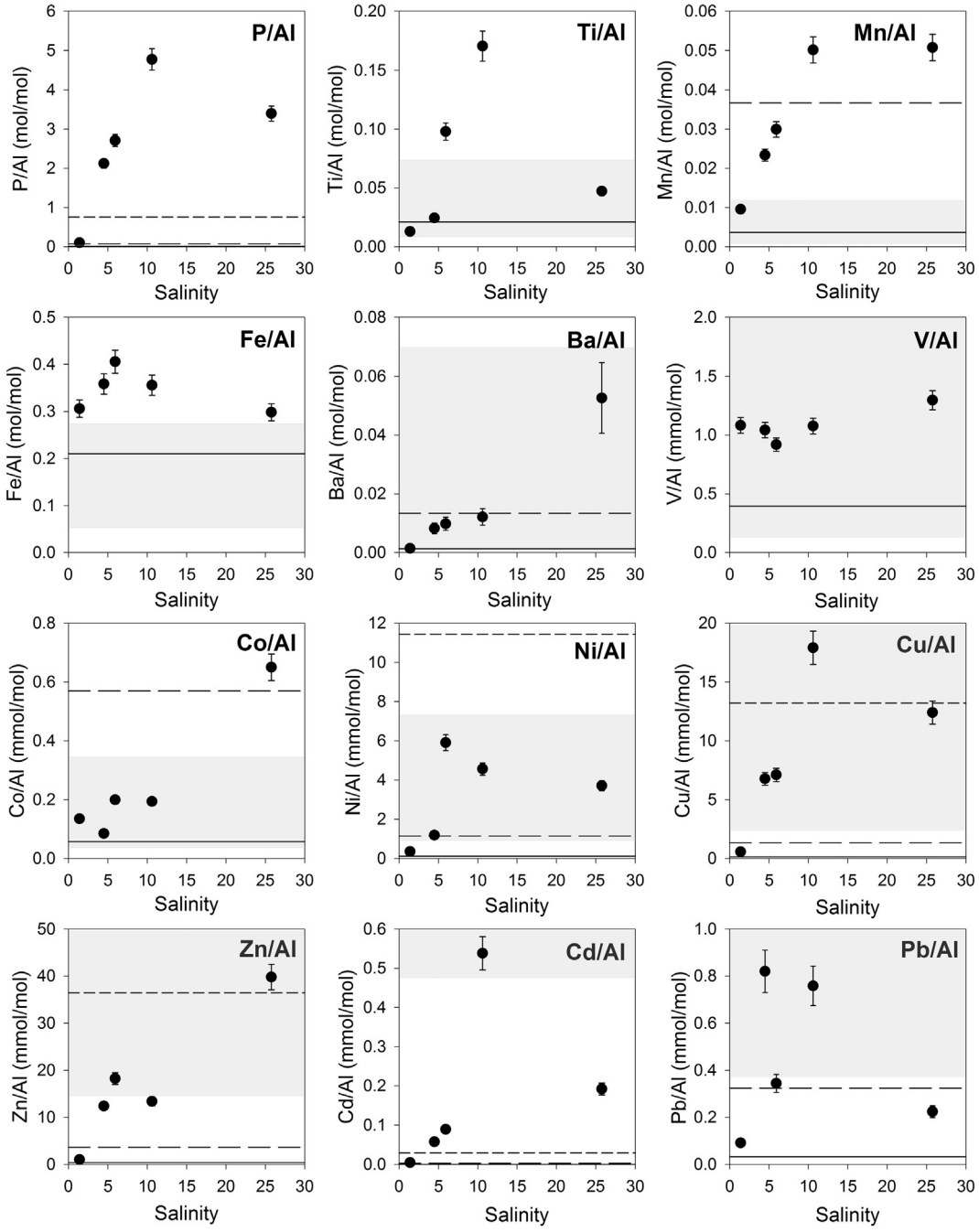

Fig. 7. Particulate TE/Al molar ratios plotted against melt pond salinity. Horizontal lines represent average UCC TE/Al (solid), 10× average UCC TE/Al (long dashes), and 100× average UCC TE/Al molar ratios (short dashes), based on Taylor and Mclennan (1995) data. TE/Al ratios are in mol/mol for P, Ti, Mn, Fe and Ba, and mmol/mol for all other elements. Gray shading indicates the range of TE/Al molar ratios measured in bulk aerosol samples collected during GN01 (Marsay et al., 2018).

correlation with salinity (Fig. 6) or with each other. Although dZn and dPb concentration variations between melt ponds were different from one another, both, like dFe, were mostly in the colloidal size fraction (Fig. 3), and both had lower concentrations than the value modeled from snow, sea ice and seawater contributions (Table 5). Thus, as proposed for dFe, we suggest that dZn and dPb could have been lost to the particulate phase within the melt ponds due to scavenging or aggregation processes. As mentioned previously, calculations based on particulate phosphorus concentrations and sea ice algal Zn/P ratios suggest that biological uptake likely removed relatively little dZn, compared to observed dZn concentrations. Melt pond dissolved δ^{66}Zn measurements were quite variable (−0.11‰ to +0.75‰; Fig. 6), highlighting the complex combination of different Zn sources and/or fractionation processes during internal cycling which govern Zn concentrations and isotope ratios in melt ponds.

Although dMn showed no correlation with salinity, its characteristics in melt ponds were in some ways similar to those of the elements that did. There was negligible (< 5%) colloidal Mn (Fig. 3), similar to the colloidal fraction in seawater and sea ice dMn (0% and 2% colloids, respectively), but much lower than snow dMn (76% colloidal) (Lanning et al., 2017). This was true even for Station 33, where snowmelt made the greatest contribution to melt pond volume. However, melt pond dMn concentrations were generally higher than those in seawater, snow or sea ice, such that measured melt pond dMn concentrations were

~150% higher, on average, than those modeled based on end-member concentrations. This is potentially due to higher concentrations of soluble Mn in wintertime aerosols and thus higher dMn in the snowmelt that initially formed the melt ponds. However, another reasonable explanation is solubilization by photoreduction of particulate Mn (Sunda et al., 1983) released into the melt ponds from snow and sea ice. As noted in the discussion of δ^{56}Fe, melt ponds receive long periods of irradiance during the Arctic summer, promoting the potential for photochemical reactions.

Dissolved Al concentrations were relatively invariant in four of the melt ponds, with significantly higher dAl at the Station 33 pond that was rich in snowmelt (Fig. 2). This mirrored the much higher pAl concentrations at that station (Fig. 4) and likely represents a higher contribution to the Station 33 melt pond from Al solubilized from particles in snow and/or sea ice. Though Al and Ga are both potential tracers of dust inputs, their dissolved concentrations had very different trends with salinity in the five melt ponds (Fig. 6). However, the dGa/dAl ratio displayed a significant correlation with salinity ($r^2 = 0.93$, $p < 0.01$), with low salinity dGa/dAl ratios closer to the crustal Ga/Al ratio and higher values at higher salinity indicative of the longer residence time of dGa in the surface seawater end-member relative to dAl (Shiller and Bairamadgi, 2006).

4.3. Melt pond particulate trace elements

Potential contributions to melt pond particulate TE concentrations, as summarized in Fig. 5, include lithogenic and anthropogenic aerosol particles deposited directly from the atmosphere or released from melting snow; sediment particles released from melting sea ice; biogenic particles released from melting sea ice, formed in situ, or introduced with seawater; particles formed in situ by authigenic precipitation; and TEs scavenged onto the exterior of pre-existing particles. Particulate TEs can also be lost from melt ponds through dissolution, through settling of material to the bottom of the melt pond, or through pond drainage. Below we use elemental ratios to infer contributions of various particulate TE sources.

4.3.1. Elemental ratios of melt pond particulate material

The element/Al ratio of a sample of natural particulate material, and how it compares to the average crustal ratio of the element to Al, is often used to evaluate the relative importance of lithogenic contributions to the sample (e.g. Buck et al., 2013; Kuss and Kremling, 1999; Shelley et al., 2015). In doing so, the element of interest is considered to be predominantly associated with lithogenic material if the element/Al ratio is within a factor of ten of the upper continental crustal (UCC) average; a convention that takes into account regional and mineralogical variations in the element/Al ratios of lithogenic material. Element/Al ratios more than a factor of ten greater than the UCC average are taken to indicate a significant non-crustal contribution for the element (Chester et al., 1993).

Using this approach, TE/Al ratios of particulate material collected from melt ponds were similar to those of aerosol and snow samples collected during GN01 (Bolt et al., manuscript in preparation; Marsay et al., 2018), and to aerosols collected in the high Arctic (> 80°N) during a previous summertime study (Kadko et al., 2016). For Fe, Ti, and V, pTE/pAl in all melt ponds and GN01 aerosol samples were within a factor of ten of UCC values (Fig. 7, using UCC composition from Taylor and McLennan (1995)). The melt pond pCo/pAl and pBa/pAl ratios were within a factor of ten of UCC values for all except the most saline pond (values were 11 times and 39 times crustal for pCo/pAl and pBa/pAl, respectively, at Station 43), while pMn/pAl was only significantly enriched in the two most saline melt ponds (~14 times UCC values at both Stations 39 and 43). Thus, for these elements (Fe, Ti, V, Co, Ba, and Mn), the melt pond particulate TE concentrations can be broadly explained by the presence of lithogenic material.

For Ni, Cu, Zn, Cd and Pb, melt pond (and aerosol) pTE/pAl ratios were generally at least a factor of ten greater than average UCC ratios, and as much as three orders of magnitude greater for Cd (Fig. 7). For these elements, the aerosol enrichments can be explained by relatively low mineral dust loading to the Arctic Ocean, due to its remoteness from natural dust sources (Mahowald et al., 2009), together with anthropogenic aerosol contributions. Anthropogenic emissions generated by fossil fuel combustion and non-ferrous metal production represent significant global contributions to aerosol production for several elements, including those listed (Pacyna and Pacyna, 2001), and these are often associated with smaller (< 1 μm) particles (Duce et al., 1991; Jang et al., 2007). These smaller aerosol particles remain in the atmosphere longer and can be transported farther than larger natural dust particles (Mahowald et al., 2005; Schulz et al., 1998), resulting in TE enrichments in remote aerosols. The melt pond particulate data are therefore consistent with an anthropogenically-influenced aerosol source, deposited either directly during the melt season or with the snowmelt that contributed to melt pond volume.

The overlap between melt pond particulate TE/Al ratios and those of summertime aerosols may be coincidental, given that the former should include material from the Arctic Haze period. Time-series data from aerosol sampling sites around the Arctic indicate little seasonal variation in mineral aerosol concentrations (from Al data), but winter/spring maxima in various pollutant elements that vary from 2 to 3 times (Cu, Zn) to a factor of ten (Pb) higher than summertime concentrations, due to the Arctic Haze phenomenon (Gong and Barrie, 2005; Laing et al., 2014; Shaw, 1995; Sirois and Barrie, 1999), resulting in corresponding seasonal trends in aerosol TE/Al ratios. Thus, snowmelt carrying atmospheric deposits from the Arctic Haze period may be expected to have higher TE/Al ratios than summertime aerosols. However, the GN01 aerosol data reveal short-term changes in TE/Al ratio that also span an order of magnitude for some elements and two orders of magnitude for Pb (Marsay et al., 2018), while the 20-year time-series of Gong and Barrie (2005) shows strong variability in aerosol TE concentrations in any given month.

Several other competing factors may also have influenced the melt pond particulate TE/Al ratios prior to their measurement during GN01. Sinking of some of the original (snowmelt-introduced) aerosol particle load to the bottom of the ponds would have resulted in that material not being sampled during this study. Secondly, dissolution of variable fractions of aerosol TEs (relative to Al) within the melt pond environment would likely change the TE/Al of the remaining material, relative to that of the source material. Aerosol TEs derived from anthropogenic sources, such as those that contribute to Arctic Haze, are typically more soluble than those in mineral aerosols (e.g. Guieu et al., 1994; Sholkovitz et al., 2009). Thus, dissolution would likely lower some TE/Al ratios in melt pond particles relative to the source aerosol due to more of the pollutant element being lost to solution than the mineral dust-associated Al. In addition, any contribution to melt pond particle load from sediment released from melting sea ice (Eicken et al., 2005; Nürnberg et al., 1994; Wegner et al., 2017) would be expected to shift pTE/pAl ratios closer to UCC ratios.

A further observation from Fig. 7 is that for several elements the TE/Al ratio of melt pond particles generally increases with increasing salinity. This suggests that the degree of seawater intrusion into melt ponds has some influence on particulate concentrations of such elements, relative to pAl concentration. This may be through particulate material being introduced to the melt ponds with seawater, or through scavenging and/or aggregation of dissolved phase TEs as seawater and freshwater sources mix. However, it is difficult to draw any strong conclusions about this trend from only five samples. Of the elements shown in Fig. 7, only Ba/Al, Co/Al and Zn/Al ratios show any statistically significant correlation (at the $p < 0.05$ level) with salinity.

4.3.2. Potential contributions from biogenic material

Previous studies have reported melt pond chlorophyll *a* concentrations spanning two orders of magnitude and similar to those in the

underlying seawater (Bates et al., 2014; Gradinger et al., 2005; Lee et al., 2012). Thus, the enrichment of certain elements observed in melt pond particles over crustal TE/Al ratios could reflect the presence of biogenic material (e.g. Kuss and Kremling, 1999). Unfortunately, neither photosynthetic pigments nor particulate organic carbon were measured in this study. Instead we investigate potential biogenic contributions to melt pond particles by consideration of non-crustal pP concentration, which is assumed to be entirely biogenic (based on the lack of an observed enrichment of P over Al relative to crustal values in Arctic aerosols (Kadko et al., 2016)).

Thus, the biogenic pP (pP_{bio}) is calculated as:

$$pP_{bio} = pP - (pAl \times \text{crustal P/Al}) \quad (1)$$

using a crustal P/Al ratio of 0.0076 mol/mol (Taylor and Mclennan, 1995). Doing so suggests that pP_{bio} contributed 92% of pP at Station 33 and > 99% at the other four stations. Non-crustal particulate concentrations for the other TEs were calculated in a similar way and the resulting non-crustal pTE/pP_{bio} molar ratios are listed in Table 6, along with the percentage contribution of non-crustal pTE to total pTE. Also shown are pTE/pP_{bio} ratios measured in algal cells collected from the sea ice at Stations 33, 42 and 43, and the range of values measured in marine phytoplankton in previous work (Twining and Baines, 2013).

The melt pond non-crustal pTE/pP_{bio} ratios for Co, Ni, Cu, Zn and Cd generally fall within the range of cellular ratios measured in sea ice samples in this study, and as previously summarized for marine plankton values. Thus, it is plausible that in most cases a biogenic fraction of particulate material could account for the non-crustal pTE concentrations of these elements, which often represented the majority of total particulate concentrations for some elements (i.e. those with significant enrichments over crustal TE/Al ratios). However, we note that our calculated non-lithogenic pP is not necessarily all associated with algal material. Although Arctic aerosols show no significant enrichment in P relative to crustal material, there could also be contributions to melt pond pP from detrital organic P introduced with ice-rafted material of marine or terrestrial origin. Such material would also, presumably, make some contribution to melt pond non-crustal pTE concentrations.

While most melt pond non-crustal pTE/pP_{bio} values in Table 6 can be broadly explained by a contribution from algal material to the particle load, the values for Mn and Fe were largely above those observed in phytoplankton, likely indicating contributions from oxyhydroxide formation and/or scavenging from the dissolved phase within the melt pond. Station 33 provides a particularly strong example of this, with notably higher pMn/pP_{bio} and pFe/pP_{bio} values, and a detrital contribution may indeed be responsible for this. Radium-228 activities measured in surface waters during GN01 reveal that all ice stations occupied were in a region influenced by the Transpolar Drift, while an ice back-trajectory analysis specifically for Station 33 indicates transport from the Laptev Sea (Kipp et al., 2018). Thus, it is feasible that the relatively small contribution from sea ice to melt pond water at Station 33 carried with it a significant particle load of shelf-derived particulate material diagenetically enriched in Fe and Mn.

At the very least, the calculated non-crustal pTE concentrations are highly dependent on the TE/Al ratios used, and these can vary significantly among different natural dust and/or sediment sources compared to average crustal values (e.g. Guieu et al., 2002; Krueger et al., 2004). Further investigation and melt pond chlorophyll *a* data would be necessary to put these data into better context.

4.4. Melt pond biogeochemistry in a changing Arctic

The Arctic region has experienced significant recent changes as a result of anthropogenic greenhouse gas emissions and regional amplification effects (Serreze and Barry, 2011; Vaughan et al., 2013). Annual sea ice extent has decreased at a rate of ~4% per decade since satellite observations began in 1979, while summertime sea ice extent has decreased at an even faster rate (Comiso, 2012; Vaughan et al., 2013). This has been accompanied by an increase in melt season length (Markus et al., 2009; Stammerjohn et al., 2012), a shift in the dominant sea ice cover from multi-year to first year ice (Comiso, 2012; Maslanik et al., 2011), and a decrease in average thickness and total volume of sea ice (Kwok et al., 2009; Laxon et al., 2013; Rothrock et al., 2008). These trends are expected to continue in the coming decades, with nearly ice-free summertime conditions predicted to occur by 2100, and possibly as early as 2030 (Kirtman et al., 2013; Overland and Wang, 2013; Stroeve et al., 2007).

Along with climate-driven changes in Arctic fluvial inputs (White et al., 2007) and precipitation patterns and frequency (Curtis et al., 1998; Liu et al., 2012; Macdonald et al., 2005), and the related changes in inputs of micronutrient and pollutant elements, these sea ice trends will likely lead to future changes in TE biogeochemical cycles in the Arctic. However, our understanding of how significant these changes may be, and whether they will have additional effects upon the Arctic ecosystem, is currently limited by the small number of TE studies carried out in the Arctic, something that the recent GEOTRACES sections aimed to address. One such uncertainty is how changes in sea ice coverage might affect the air-sea transfer of TEs and their availability to primary producers.

The sea ice environment represents a dynamic link between the atmosphere, cryosphere, and surface ocean that is unique to the polar regions. Melt ponds represent an important feature of the Arctic sea ice regime, and our salinity, $\delta^{18}O$, and ^{7}Be data demonstrate the complex connections between melt ponds and the atmosphere, sea ice, and seawater. Our small dataset represents a snapshot of melt pond trace element biogeochemistry from late summer/early fall and cannot answer all of the questions about the role that melt ponds play in modulating the input and bioavailability of atmospheric deposition to Arctic Ocean surface waters. However, our data reveal some of the different controls on dissolved and particulate TEs in melt ponds, and can provide a guide for future studies of trace element biogeochemistry during the evolution of these transient features.

The salinity, $\delta^{18}O$, and ^{7}Be data from the five melt ponds studied reveal varying degrees of influence by melting of the surrounding sea ice, and exchange with the underlying water column, as well as snowmelt, and these sources had varying degrees of importance for the different TEs measured. For some elements (V, Ni, Cu, Cd, Ba, and possibly Co), the dissolved phase concentrations were dominated by the influence of seawater intrusion to the ponds, which suggests that the seasonal release of these elements from draining melt ponds does not play a major role in their surface ocean distributions in the Arctic Ocean, despite several of these elements having large anthropogenic aerosol contributions during the Arctic Haze period. Thus, we suggest that changes in seasonality and extent of sea ice coverage may not significantly affect surface ocean concentrations of these elements.

For other trace elements (Al, Mn, Fe, Zn, Pb, and possibly Ga), there was no single clear control on the dissolved TE concentrations, or there was evidence of the importance of atmospheric deposition. Comparison of dFe, dZn and dPb concentrations measured in melt ponds to those expected based on content of the three source reservoirs suggest a loss of these elements from the dissolved phase within melt ponds. This may be linked to the relatively high contributions of colloids to dissolved concentrations of these elements in each source water, which may facilitate aggregation and scavenging as different sources mix in the melt ponds. In contrast, melt pond dMn was higher than calculated based on end-members, suggesting a significant release from particulate material within the ponds. This indicates a role for melt ponds in modifying atmospheric inputs of these elements before they are introduced to the surface ocean. Thus, the shift towards seasonal and less extensive ice coverage, thinner ice and earlier melting is likely to influence the bioavailability of each of these elements in surface waters, by reducing the amount of material “processed” through melt ponds before delivery to the surface ocean.

Acknowledgements

This research was supported by National Science Foundation awards OCE-1438047 to CSB, OCE-1437266 to WML, OCE-1433717 to AA and Rob Rember, OCE-1434493 to JNF and RMS, OCE-1713677 to JNF, OCE-1434085 to DK, OCE-1436019 to PLM, OCE-1439253 to Chris Measures and MH, OCE-1436312 to AMS, and OCE-1435862 to BST. Oxygen isotope work was supported by NSF awards OCE-1436666 and GG008984-01 to Peter Schlosser. AA was also funded by BOEM through University of Alaska Coastal Marine Institute contract number M13 AC00002. A portion of this work was performed at the National High Magnetic Field Laboratory, which is supported by NSF Cooperative Agreement # DMR-1157490 and the State of Florida. Thanks to Lee Ann DeLeo at SkIO for her work on Fig. 3. The authors gratefully acknowledge Rob Rember, Gabi Weiss and Neil Wyatt for their assistance with collection and shipboard processing of melt pond TE samples, Mark Stephens and Paul Aguilar for their assistance with ^{7}Be sample collections and analysis, and members of the Oceanographic Data Facility of Scripps Institute of Oceanography for analysis of salinity samples. Thanks also to the officers and crew of the USCGC *Healy* for their support during the US GEOTRACES GN01 expedition.

Appendix A. Supplementary data

Supplementary data to this article can be found online at https://doi.org/10.1016/j.marchem.2018.06.002.

References

Aguilar-Islas, A.M., Rember, R.D., 2017. Trace metal concentrations in the sea ice environment during the US GEOTRACES Arctic section. In: ASLO 2017 Aquatic. Sci. Meet., Honolulu, HI, (Abstract #30135).

Aspmo, K., Temme, C., Berg, T., Ferrari, C., Gauchard, P.-A., Fain, X., Wibetoe, G., 2006. Mercury in the atmosphere, snow and melt water ponds in the North Atlantic Ocean during Arctic summer. Environ. Sci. Technol. 40, 4083–4089. http://dx.doi.org/10.1021/es052117z.

Barrie, L.A., Hoff, R.M., 1985. Five years of air chemistry observations in the Canadian Arctic. Atmos. Environ. 19, 1995–2010. http://dx.doi.org/10.1016/0004-6981(85)90108-8.

Bates, N.R., Garley, R., Frey, K.E., Shake, K.L., Mathis, J.T., 2014. Sea-ice melt CO_2-carbonate chemistry in the western Arctic Ocean: meltwater contributions to air-sea CO_2 gas exchange, mixed-layer properties and rates of net community production under sea ice. Biogeosciences 11, 6769–6789. http://dx.doi.org/10.5194/bg-11-6769-2014.

Beard, B.L., Johnson, C.M., Von Damm, K.L., Poulson, R.L., 2003. Iron isotope constraints on Fe cycling and mass balance in oxygenated Earth oceans. Geology 31, 629–632. http://dx.doi.org/10.1130/0091-7613(2003)031<0629:IICOFC>2.0.CO;2.

Bolt, C., Rember, R., Aguilar-Islas, A., (manuscript in preparation) Distribution and reactivity of particulate trace elements in snow and sea ice during US GEOTRACES Western Arctic cruise GN01.

Buck, C.S., Landing, W.M., Resing, J., 2013. Pacific Ocean aerosols: deposition and solubility of iron, aluminum, and other trace elements. Mar. Chem. 157, 117–130. http://dx.doi.org/10.1016/j.marchem.2013.09.005.

Chester, R., Murphy, K.J.T., Lin, F.J., Berry, A.S., Bradshaw, G.A., Corcoran, P.A., 1993. Factors controlling the solubilities of trace metals from non-remote aerosols deposited to the sea surface by the "dry" deposition mode. Mar. Chem. 42, 107–126. http://dx.doi.org/10.1016/0304-4203(93)90241-F.

Comiso, J.C., 2012. Large decadal decline of the Arctic multiyear ice cover. J. Clim. 25, 1176–1193. http://dx.doi.org/10.1175/JCLI-D-11-00113.1.

Conway, T.M., John, S.G., 2014. Quantification of dissolved iron sources to the North Atlantic Ocean. Nature 511, 212–215. http://dx.doi.org/10.1038/nature13482.

Conway, T.M., John, S.G., 2015. The cycling of iron, zinc and cadmium in the North East Pacific Ocean - insights from stable isotopes. Geochim. Cosmochim. Acta 164, 262–283. http://dx.doi.org/10.1016/j.gca.2015.05.023.

Conway, T.M., Rosenberg, A.D., Adkins, J.F., John, S.G., 2013. A new method for precise determination of iron, zinc and cadmium stable isotope ratios in seawater by double-spike mass spectrometry. Anal. Chim. Acta 793, 44–52. http://dx.doi.org/10.1016/j.aca.2013.07.025.

Curry, J.A., Schramm, J.L., Ebert, E.E., 1995. Sea ice-albedo climate feedback mechanism. J. Clim. 8, 240–247. http://dx.doi.org/10.1175/1520-0442(1995)008<0240:Siacfm>2.0.Co;2.

Curtis, J., Wendler, G., Stone, R., Dutton, E., 1998. Precipitation decrease in the western Arctic, with special emphasis on Barrow and Barter Island, Alaska. Int. J. Climatol. 18, 1687–1707. http://dx.doi.org/10.1002/(SICI)1097-0088(199812)18:15<1687::AID-JOC341>3.0.CO;2-2.

Darby, D.A., Burckle, L.H., Clark, D.L., 1974. Airborne dust on the Arctic pack ice, its composition and fallout rate. Earth Planet. Sci. Lett. 24, 166–172. http://dx.doi.org/10.1016/0012-821X(74)90093-4.

de Jong, J., Schoemann, V., Tison, J.-L., Becquevort, S., Masson, F., Lannuzel, D., Petit, J., Chou, L., Weis, D., Mattielli, N., 2007. Precise measurement of Fe isotopes in marine samples by multi-collector inductively coupled plasma mass spectrometry (MC-ICP-MS). Anal. Chim. Acta 589, 105–119. http://dx.doi.org/10.1016/j.aca.2007.02.055.

Duce, R.A., Liss, P.S., Merrill, J.T., Atlas, E.L., Buat-Menard, P., Hicks, B.B., Miller, J.M., Prospero, J.M., Arimoto, R., Church, T.M., Ellis, W., Galloway, J.N., Hansen, L., Jickells, T.D., Knap, A.H., Reinhardt, K.H., Schneider, B., Soudine, A., Tokos, J.J., Tsunogai, S., Wollast, R., Zhou, M., 1991. The atmospheric input of trace species to the world ocean. Glob. Biogeochem. Cycles 5, 193–259. http://dx.doi.org/10.1029/91GB01778.

Eicken, H., Krouse, H.R., Kadko, D., Perovich, D.K., 2002. Tracer studies of pathways and rates of meltwater transport through Arctic summer sea ice. J. Geophys. Res. Ocean 107, 8046. http://dx.doi.org/10.1029/2000JC000583.

Eicken, H., Grenfell, T.C., Perovich, D.K., Richter-Menge, J.A., Frey, K., 2004. Hydraulic controls of summer Arctic pack ice albedo. J. Geophys. Res. Ocean 109, C08007. http://dx.doi.org/10.1029/2003JC001989.

Eicken, H., Gradinger, R., Gaylord, A., Mahoney, A., Rigor, I., Melling, H., 2005. Sediment transport by sea ice in the Chukchi and Beaufort Seas: increasing importance due to changing ice conditions? Deep Sea Res. Part II Top. Stud. Oceanogr. 52, 3281–3302. http://dx.doi.org/10.1016/j.dsr2.2005.10.006.

Ellwood, M.J., Hutchins, D.A., Lohan, M.C., Milne, A., Nasemann, P., Nodder, S.D., Sander, S.G., Strzepek, R., Wilhelm, S.W., Boyd, P.W., 2015. Iron stable isotopes track pelagic iron cycling during a subtropical phytoplankton bloom. Proc. Natl. Acad. Sci. 112, E15–E20. http://dx.doi.org/10.1073/pnas.1421576112.

Escoube, R., Rouxel, O.J., Sholkovitz, E., Donard, O.F.X., 2009. Iron isotope systematics in estuaries: the case of North River, Massachusetts (USA). Geochim. Cosmochim. Acta 73, 4045–4059. http://dx.doi.org/10.1016/j.gca.2009.04.026.

Fernández-Méndez, M., Wenzhöfer, F., Peeken, I., Sørensen, H.L., Glud, R.N., Boetius, A., 2014. Composition, buoyancy regulation and fate of ice algal aggregates in the central Arctic Ocean. PLoS One 9. http://dx.doi.org/10.1371/journal.pone.0107452.

Fernández-Méndez, M., Katlein, C., Rabe, B., Nicolaus, M., Peeken, I., Bakker, K., Flores, H., Boetius, A., 2015. Photosynthetic production in the central Arctic Ocean during the record sea-ice minimum in 2012. Biogeosciences 12, 3525–3549. http://dx.doi.org/10.5194/bg-12-3525-2015.

Fetterer, F., Untersteiner, N., 1998. Observations of melt ponds on Arctic sea ice. J. Geophys. Res. Ocean 103, 24,821–24,835. http://dx.doi.org/10.1029/98JC02034.

Fitzsimmons, J.N., Boyle, E.A., 2014. Assessment and comparison of Anopore and cross flow filtration methods for the determination of dissolved iron size fractionation into soluble and colloidal phases in seawater. Limnol. Oceanogr. Methods 12, 246–263. http://dx.doi.org/10.4319/lom.2014.12.246.

Gong, S.L., Barrie, L.A., 2005. Trends of heavy metal components in the Arctic aerosols and their relationship to the emissions in the Northern Hemisphere. Sci. Total Environ. 342, 175–183. http://dx.doi.org/10.1016/j.scitotenv.2004.12.031.

Gradinger, R.R., Meiners, K., Plumley, G., Zhang, Q., Bluhm, B.A., 2005. Abundance and composition of the sea-ice meiofauna in off-shore pack ice of the Beaufort Gyre in summer 2002 and 2003. Polar Biol. 28, 171–181. http://dx.doi.org/10.1007/s00300-004-0674-5.

Guieu, C., Duce, R., Arimoto, R., 1994. Dissolved input of manganese to the ocean: aerosol source. J. Geophys. Res. Atmos. 99, 18,789–18,800. http://dx.doi.org/10.1029/94JD01120.

Guieu, C., Loÿe-Pilot, M.D., Ridame, C., Thomas, C., 2002. Chemical characterization of the Saharan dust end-member: some biogeochemical implications for the western Mediterranean Sea. J. Geophys. Res. Atmos. 107, 4528. http://dx.doi.org/10.1029/2001JD000582.

Hathorne, E.C., Haley, B., Stichel, T., Grasse, P., Zieringer, M., Frank, M., 2012. Online preconcentration ICP-MS analysis of rare earth elements in seawater. Geochem. Geophys. Geosyst. 13 (Q01020). http://dx.doi.org/10.1029/2011GC003907.

Jacquet, S.H.M., Dehairs, F., Cardinal, D., Navez, J., Delille, B., 2005. Barium distribution across the Southern Ocean frontal system in the Crozet-Kerguelen Basin. Mar. Chem. 95, 149–162. http://dx.doi.org/10.1016/j.marchem.2004.09.002.

Jang, H.-N., Seo, Y.-C., Lee, J.-H., Hwang, K.-W., Yoo, J.-I., Sok, C.-H., Kim, S.-H., 2007. Formation of fine particles enriched by V and Ni from heavy oil combustion: anthropogenic sources and drop-tube furnace experiments. Atmos. Environ. 41, 1053–1063. http://dx.doi.org/10.1016/j.atmosenv.2006.09.011.

Janssens, J., Meiners, K.M., Tison, J.-L., Dieckmann, G., Delille, B., Lannuzel, D., 2016. Incorporation of iron and organic matter into young Antarctic sea ice during its initial growth stages. Elem. Sci. Anthr. 4. http://dx.doi.org/10.12952/journal.elementa.000123.

Jickells, T., Moore, C.M., 2015. The importance of atmospheric deposition for ocean productivity. Annu. Rev. Ecol. Evol. Syst. 46, 481–501. http://dx.doi.org/10.1146/annurev-ecolsys-112414-054118.

John, S.G., Kunzmann, M., Townsend, E.J., Rosenberg, A.D., 2017. Zinc and cadmium stable isotopes in the geological record: a case study from the post-snowball Earth Nuccaleena cap dolostone. Palaeogeogr. Palaeoclimatol. Palaeoecol. 466, 202–208. http://dx.doi.org/10.1016/j.palaeo.2016.11.003.

Kadko, D., 2000. Modeling the evolution of the Arctic mixed layer during the fall 1997 Surface Heat Budget of the Arctic Ocean (SHEBA) Project using measurements of ^{7}Be. J. Geophys. Res. Ocean 105, 3369–3378. http://dx.doi.org/10.1029/1999JC900311.

Kadko, D., Swart, P., 2004. The source of the high heat and freshwater content of the upper ocean at the SHEBA site in the Beaufort Sea in 1997. J. Geophys. Res. Ocean 109, C01022. http://dx.doi.org/10.1029/2002JC001734.

Kadko, D., Galfond, B., Landing, W.M., Shelley, R.U., 2016. Determining the pathways, fate, and flux of atmospherically derived trace elements in the Arctic ocean/ice system. Mar. Chem. 182, 38–50. http://dx.doi.org/10.1016/j.marchem.2016.04.006.

Kipp, L.E., Charette, M.A., Moore, W.S., Henderson, P.B., Rigor, I.G., 2018. Increased

fluxes of shelf-derived materials to the central Arctic Ocean. Sci. Adv. 4, eaao1302. http://dx.doi.org/10.1126/sciadv.aao1302.
Kirtman, B., Power, S.B., Adedoyin, J.A., Boer, G.J., Bojariu, R., Camilloni, I., Doblas-Reyes, F.J., Fiore, A.M., Kimoto, M., Meehl, G.A., Prather, M., Sarr, A., Schär, C., Sutton, R., van Oldenborgh, G.J., Vecchi, G., Wang, H.J., 2013. Near-term Climate Change: Projections and Predictability. In: Stocker, T.F., Qin, D., Plattner, G.-K., Tignor, M., Allen, S.K., Boschung, J., Nauels, A., Xia, Y., Bex, V., Midgley, P.M. (Eds.), Climate Change 2013: The Physical Science Basis. Contribution of Working Group I to the Fifth Assessment Report of the Intergovernmental Panel on Climate Change. Cambridge University Press, Cambridge, UK and New York, NY, USA.
Krueger, B.J., Grassian, V.H., Cowin, J.P., Laskin, A., 2004. Heterogeneous chemistry of individual mineral dust particles from different dust source regions: the importance of particle mineralogy. Atmos. Environ. 38, 6253–6261. http://dx.doi.org/10.1016/j.atmosenv.2004.07.010.
Kuss, J., Kremling, K., 1999. Spatial variability of particle associated trace elements in near-surface waters of the North Atlantic (30°N/60°W to 60°N/2°W), derived by large volume sampling. Mar. Chem. 68, 71–86. http://dx.doi.org/10.1016/S0304-4203(99)00066-3.
Kwok, R., Cunningham, G.F., Wensnahan, M., Rigor, I., Zwally, H.J., Yi, D., 2009. Thinning and volume loss of the Arctic Ocean sea ice cover: 2003–2008. J. Geophys. Res. Ocean 114, C07005. http://dx.doi.org/10.1029/2009JC005312.
Lagerström, M.E., Field, M.P., Séguret, M., Fischer, L., Hann, S., Sherrell, R.M., 2013. Automated on-line flow-injection ICP-MS determination of trace metals (Mn, Fe, Co, Ni, Cu and Zn) in open ocean seawater: application to the GEOTRACES program. Mar. Chem. 155, 71–80. http://dx.doi.org/10.1016/j.marchem.2013.06.001.
Laing, J.R., Hopke, P.K., Hopke, E.F., Husain, L., Dutkiewicz, V.A., Paatero, J., Viisanen, Y., 2014. Long-term particle measurements in Finnish Arctic: part I - chemical composition and trace metal solubility. Atmos. Environ. 88, 275–284. http://dx.doi.org/10.1016/j.atmosenv.2014.03.002.
Lanning, N.T., Jensen, L.T., Sherrell, R.M., Fitzsimmons, J.N., 2017. Size partitioning of dissolved trace metals into soluble and colloidal fractions in sea ice, snow and melt ponds of the western Arctic Ocean. In: ASLO 2017 Aquatic. Sci. Meet., Honolulu, HI, (Abstract #28970).
Lannuzel, D., Vancoppenolle, M., van der Merwe, P., de Jong, J., Meiners, K.M., Grotti, M., Nishioka, J., Schoemann, V., 2016. Iron in sea ice: review and new insights. Elem. Sci. Anthr. 4 (130). http://dx.doi.org/10.12952/journal.elementa.000130.
Laxon, S.W., Giles, K.A., Ridout, A.L., Wingham, D.J., Willatt, R., Cullen, R., Kwok, R., Schweiger, A., Zhang, J., Haas, C., Hendricks, S., Krishfield, R., Kurtz, N., Farrell, S., Davidson, M., 2013. CryoSat-2 estimates of Arctic sea ice thickness and volume. Geophys. Res. Lett. 40, 732–737. http://dx.doi.org/10.1002/grl.50193.
Lee, S.H., Stockwell, D.A., Joo, H.-M., Son, Y.B., Kang, C.-K., Whitledge, T.E., 2012. Phytoplankton production from melting ponds on Arctic sea ice. J. Geophys. Res. Ocean 117, C04030. http://dx.doi.org/10.1029/2011JC007717.
Liu, J., Curry, J.A., Wang, H., Song, M., Horton, R.M., 2012. Impact of declining Arctic sea ice on winter snowfall. Proc. Natl. Acad. Sci. 109, 4074–4079. http://dx.doi.org/10.1073/pnas.1114910109.
Lüthje, M., Feltham, D.L., Taylor, P.D., Worster, M.G., 2006. Modeling the summertime evolution of sea-ice melt ponds. J. Geophys. Res. Ocean 111, C02001. http://dx.doi.org/10.1029/2004JC002818.
Macdonald, R.W., Harner, T., Fyfe, J., 2005. Recent climate change in the Arctic and its impact on contaminant pathways and interpretation of temporal trend data. Sci. Total Environ. 342, 5–86. http://dx.doi.org/10.1016/j.scitotenv.2004.12.059.
Mahowald, N.M., Baker, A.R., Bergametti, G., Brooks, N., Duce, R.A., Jickells, T.D., Kubilay, N., Prospero, J.M., Tegen, I., 2005. Atmospheric global dust cycle and iron inputs to the ocean. Glob. Biogeochem. Cycles 19, GB4025. http://dx.doi.org/10.1029/2004GB002402.
Mahowald, N.M., Engelstaedter, S., Luo, C., Sealy, A., Artaxo, P., Benitez-Nelson, C., Bonnet, S., Chen, Y., Chuang, P.Y., Cohen, D.D., Dulac, F., Herut, B., Johansen, A.M., Kubilay, N., Losno, R., Maenhaut, W., Paytan, A., Prospero, J.M., Shank, L.M., Siefert, R.L., 2009. Atmospheric iron deposition: global distribution, variability, and human perturbations. Annu. Rev. Mar. Sci. 1, 245–278. http://dx.doi.org/10.1146/annurev.marine.010908.163727.
Markus, T., Stroeve, J.C., Miller, J., 2009. Recent changes in Arctic sea ice melt onset, freezeup, and melt season length. J. Geophys. Res. Ocean 114, C12024. http://dx.doi.org/10.1029/2009JC005436.
Marsay, C.M., Kadko, D., Landing, W.M., Morton, P.L., Summers, B.A., Buck, C.S., 2018. Concentrations, provenance and flux of aerosol trace elements during US GEOTRACES western Arctic cruise GN01. Chem. Geol. http://dx.doi.org/10.1016/j.chemgeo.2018.06.007. (in press).
Maslanik, J., Stroeve, J., Fowler, C., Emery, W., 2011. Distribution and trends in Arctic sea ice age through spring 2011. Geophys. Res. Lett. 38, L13502. http://dx.doi.org/10.1029/2011GL047735.
Measures, C., Hatta, M., Fitzsimmons, J., Morton, P., 2015. Dissolved Al in the zonal N Atlantic section of the US GEOTRACES 2010/2011 cruises and the importance of hydrothermal inputs. Deep Sea Res. Part II Top. Stud. Oceanogr. 116, 176–186. http://dx.doi.org/10.1016/j.dsr2.2014.07.006.
Melnikov, I.A., Kolosova, E.G., Welch, H.E., Zhitina, L.S., 2002. Sea ice biological communities and nutrient dynamics in the Canada Basin of the Arctic Ocean. Deep Sea Res. Part I Oceanogr. Res. Pap. 49, 1623–1649. http://dx.doi.org/10.1016/S0967-0637(02)00042-0.
Milne, A., Landing, W., Bizimis, M., Morton, P., 2010. Determination of Mn, Fe, Co, Ni, Cu, Zn, Cd and Pb in seawater using high resolution magnetic sector inductively coupled mass spectrometry (HR-ICP-MS). Anal. Chim. Acta 665, 200–207. http://dx.doi.org/10.1016/j.aca.2010.03.027.
Nürnberg, D., Wollenburg, I., Dethleff, D., Eicken, H., Kassens, H., Letzig, T., Reimnitz, E., Thiede, J., 1994. Sediments in Arctic sea ice: implications for entrainment, transport and release. Mar. Geol. 119, 185–214. http://dx.doi.org/10.1016/0025-3227(94)90181-3.
Overland, J.E., Wang, M., 2013. When will the summer Arctic be nearly sea ice free? Geophys. Res. Lett. 40, 2097–2101. http://dx.doi.org/10.1002/grl.50316.
Pacyna, J.M., Pacyna, E.G., 2001. An assessment of global and regional emissions of trace metals to the atmosphere from anthropogenic sources worldwide. Environ. Rev. 9, 269–298. http://dx.doi.org/10.1139/er-9-4-269.
Pasqualini, A., Schlosser, P., Newton, R., Koffman, T.N., 2017. U.S. GEOTRACES Arctic Section Ocean Water Hydrogen and Oxygen Stable Isotope Analyses (Version 1.0) [Data set]. http://dx.doi.org/10.1594/ieda/100633.
Perovich, D.K., Grenfell, T.C., Light, B., Hobbs, P.V., 2002. Seasonal evolution of the albedo of multiyear Arctic sea ice. J. Geophys. Res. Ocean 107, 8044. http://dx.doi.org/10.1029/2000JC000438.
Perovich, D.K., Jones, K.F., Light, B., Eicken, H., Markus, T., Stroeve, J., Lindsay, R., 2011. Solar partitioning in a changing Arctic sea-ice cover. Ann. Glaciol. 52, 192–196. http://dx.doi.org/10.3189/172756411795931543.
Polashenski, C., Perovich, D., Courville, Z., 2012. The mechanisms of sea ice melt pond formation and evolution. J. Geophys. Res. Ocean 117, C01001. http://dx.doi.org/10.1029/2011JC007231.
Polashenski, C., Golden, K.M., Perovich, D.K., Skyllingstad, E., Arnsten, A., Stwertka, C., Wright, N., 2017. Percolation blockage: a process that enables melt pond formation on first year Arctic sea ice. J. Geophys. Res. Ocean 122, 413–440. http://dx.doi.org/10.1002/2016JC011994.
Resing, J.A., Measures, C.I., 1994. Fluorometric determination of Al in seawater by flow injection analysis with in-line preconcentration. Anal. Chem. 66, 4105–4111. http://dx.doi.org/10.1021/ac00094a039.
Rösel, A., Kaleschke, L., 2012. Exceptional melt pond occurrence in the years 2007 and 2011 on the Arctic sea ice revealed from MODIS satellite data. J. Geophys. Res. Ocean 117, C05018. http://dx.doi.org/10.1029/2011JC007869.
Rothrock, D.A., Percival, D.B., Wensnahan, M., 2008. The decline in Arctic sea-ice thickness: separating the spatial, annual, and interannual variability in a quarter century of submarine data. J. Geophys. Res. Ocean 113, C05003. http://dx.doi.org/10.1029/2007JC004252.
Sankelo, P., Haapala, J., Heiler, I., Rinne, E., 2010. Melt pond formation and temporal evolution at the drifting station Tara during summer 2007. Polar Res. 29, 311–321. http://dx.doi.org/10.1111/j.1751-8369.2010.00161.x.
Schulz, M., Balkanski, Y.J., Guelle, W., Dulac, F., 1998. Role of aerosol size distribution and source location in a three-dimensional simulation of a Saharan dust episode tested against satellite-derived optical thickness. J. Geophys. Res. Atmos. 103, 10,579–10,592. http://dx.doi.org/10.1029/97JD02779.
Serreze, M.C., Barry, R.G., 2011. Processes and impacts of Arctic amplification: a research synthesis. Glob. Planet. Chang. 77, 85–96. http://dx.doi.org/10.1016/j.gloplacha.2011.03.004.
Shaw, G.E., 1995. The Arctic haze phenomenon. Bull. Am. Meteorol. Soc. 76, 2403–2413. http://dx.doi.org/10.1175/1520-0477(1995)076<2403:TAHP>2.0.CO;2.
Shelley, R.U., Morton, P.L., Landing, W.M., 2015. Elemental ratios and enrichment factors in aerosols from the US-GEOTRACES North Atlantic transects. Deep Sea Res. Part II Top. Stud. Oceanogr. 116, 262–272. http://dx.doi.org/10.1016/j.dsr2.2014.12.005.
Shiller, A.M., Bairamadgi, G.R., 2006. Dissolved gallium in the northwest Pacific and the south and central Atlantic Oceans: Implications for aeolian Fe input and a re-consideration of profiles. Geochem. Geophys. Geosyst. 7 (Q08M09). http://dx.doi.org/10.1029/2005GC001118.
Sholkovitz, E.R., Sedwick, P.N., Church, T.M., 2009. Influence of anthropogenic combustion emissions on the deposition of soluble aerosol iron to the ocean: empirical estimates for island sites in the North Atlantic. Geochim. Cosmochim. Acta 73, 3981–4003. http://dx.doi.org/10.1016/j.gca.2009.04.029.
Sirois, A., Barrie, L.A., 1999. Arctic lower tropospheric aerosol trends and composition at Alert, Canada: 1980–1995. J. Geophys. Res. Atmos. 104, 11,599–11,618. http://dx.doi.org/10.1029/1999JD900077.
Sohrin, Y., Urushihara, S., Nakatsuka, S., Kono, T., Higo, E., Minami, T., Norisuye, K., Umetani, S., 2008. Multielemental determination of GEOTRACES key trace metals in seawater by ICPMS after preconcentration using an ethylenediaminetriacetic acid chelating resin. Anal. Chem. 80, 6267–6273. http://dx.doi.org/10.1021/ac800500f.
Sørensen, H.L., Thamdrup, B., Jeppesen, E., Rysgaard, S., Glud, R.N., 2017. Nutrient availability limits biological production in Arctic sea ice melt ponds. Polar Biol. 40, 1593–1606. http://dx.doi.org/10.1007/s00300-017-2082-7.
Stammerjohn, S., Massom, R., Rind, D., Martinson, D., 2012. Regions of rapid sea ice change: an inter-hemispheric seasonal comparison. Geophys. Res. Lett. 39, L06501. http://dx.doi.org/10.1029/2012GL050874.
Stroeve, J., Holland, M.M., Meier, W., Scambos, T., Serreze, M., 2007. Arctic sea ice decline: faster than forecast. Geophys. Res. Lett. 34, L09501. http://dx.doi.org/10.1029/2007GL029703.
Ström, J., Umegård, J., Tørseth, K., Tunved, P., Hansson, H.-C., Holmén, K., Wismann, V., Herber, A., König-Langlo, G., 2003. One year of particle size distribution and aerosol chemical composition measurements at the Zeppelin Station, Svalbard, March 2000-March 2001. Phys. Chem. Earth 28, 1181–1190. http://dx.doi.org/10.1016/j.pce.2003.08.058.
Sunda, W.G., Huntsman, S.A., Harvey, G.R., 1983. Photoreduction of manganese oxides in seawater and its geochemical and biological implications. Nature 301, 234–236. http://dx.doi.org/10.1038/301234a0.
Taylor, S.R., McLennan, S.M., 1995. The geochemical evolution of the continental crust. Rev. Geophys. 33, 241–265. http://dx.doi.org/10.1029/95RG00262.
Tunved, P., Ström, J., Krejci, R., 2013. Arctic aerosol life cycle: linking aerosol size distributions observed between 2000 and 2010 with air mass transport and precipitation at Zeppelin station, Ny-Ålesund, Svalbard. Atmos. Chem. Phys. 13, 3643–3660. http://dx.doi.org/10.5194/acp-13-3643-2013.

Twining, B.S., Baines, S.B., 2013. The trace metal composition of marine phytoplankton. Annu. Rev. Mar. Sci. 5, 191–215. http://dx.doi.org/10.1146/annurev-marine-121211-172322.

Twining, B.S., Rauschenberg, S., Morton, P.L., Ohnemus, D.C., Lam, P.J., 2015. Comparison of particulate trace element concentrations in the North Atlantic Ocean as determined with discrete bottle sampling and in situ pumping. Deep Sea Res. Part II Top. Stud. Oceanogr. 116, 273–282. http://dx.doi.org/10.1016/j.dsr2.2014.11.005.

Vaughan, D.G., Comiso, J.C., Allison, I., Carrasco, J., Kaser, G., Kwok, R., Mote, P., Murray, T., Paul, F., Ren, J., Rignot, E., Solomina, O., Steffen, K., Zhang, T., 2013. Observations: Cryosphere. In: Stocker, T.F., Qin, D., Plattner, G.-K., Tignor, M., Allen, S.K., Boschung, J., Nauels, A., Xia, Y., Bex, V., Midgley, P.M. (Eds.), Climate Change 2013: The Physical Science Basis. Contribution of Working Group I to the Fifth Assessment Report of the Intergovernmental Panel on Climate Change. Cambridge University Press, Cambridge, UK and New York, NY, USA.

Walker, S.A., Azetsu-Scott, K., Normandeau, C., Kelley, D.E., Friedrich, R., Newton, R., Schlosser, P., McKay, J.L., Abdi, W., Kerrigan, E., Craig, S.E., Wallace, D.W.R., 2016. Oxygen isotope measurements of seawater ($H_2{}^{18}O/H_2{}^{16}O$): a comparison of cavity ring-down spectroscopy (CRDS) and isotope ratio mass spectrometry (IRMS). Limnol. Oceanogr. Methods 14, 31–38. http://dx.doi.org/10.1002/lom3.10067.

Wegner, C., Wittbrodt, K., Hölemann, J.A., Janout, M.A., Krumpen, T., Selyuzhenok, V., Novikhin, A., Polyakova, Y., Krykova, I., Kassens, H., Timokhov, L., 2017. Sediment entrainment into sea ice and transport in the Transpolar Drift: a case study from the Laptev Sea in winter 2011/2012. Cont. Shelf Res. 141, 1–10. http://dx.doi.org/10.1016/j.csr.2017.04.010.

Welch, S.A., Beard, B.L., Johnson, C.M., Braterman, P.S., 2003. Kinetic and equilibrium Fe isotope fractionation between aqueous Fe(II) and Fe(III). Geochim. Cosmochim. Acta 67, 4231–4250. http://dx.doi.org/10.1016/S0016-7037(03)00266-7.

White, D., Hinzman, L., Alessa, L., Cassano, J., Chambers, M., Falkner, K., Francis, J., Gutowski, W.J., Holland, M., Max Holmes, R., Huntington, H., Kane, D., Kliskey, A., Lee, C., McClelland, J., Peterson, B., Rupp, T.S., Straneo, F., Steele, M., Woodgate, R., Yang, D., Yoshikawa, K., Zhang, T., 2007. The Arctic freshwater system: changes and impacts. J. Geophys. Res. Biogeosci. 112 (G04S54). http://dx.doi.org/10.1029/2006JGO00353.